MEMÓRIAS
DA
ACADEMIA DAS CIÊNCIAS
DE
LISBOA

CLASSE DE CIÊNCIAS

# Rare Earths: Not So Rare But Many Are Critical

Carlos F. G. G. Geraldes

ACADEMIA DAS CIÊNCIAS
DE LISBOA

LISBOA • 2023

*Título:* Rare Earths: Not So Rare But Many Are Critical

*Edição:* Academia das Ciências de Lisboa

*Data de edição:* 2023

# Rare Earths: Not So Rare But Many Are Critical

Carlos F. G. G. Geraldes[1,2]

**RESUMO**

As terras raras constituem um grupo de 17 elementos, os lantanóides e o escândio e ítrio, que cobrem a linha do bloco f da Tabela Periódica. Tiveram uma descoberta muito complexa devido à semelhança da sua natureza química. A sua abundância na crosta terrestre mostra que não são elementos raros, mas estando os seus depósitos principais a a sua produção mundial concentrados na China, eles são estratégicos para as necessidades tecnológicas das nações ocidentais. Embora os elementos mais leves sejam os mais abundantes, são os mais pesados que têm as aplicações mais importantes, o que torna estes elementos críticos. Uma solução para este problema é a sua reciclagem. A sub-camada electrónica 4f, com 0 a 14 electrões, é responsável pelas propriedades químicas semelhantes, dominadas pelo estado de oxidação 3+. Os fundamentos da sua química de coordenação e efeitos catalíticos são descritos, assim como as suas propriedades magnéticas e luminescentes, fundamentais para a manufactura de muitos produtos cruciais de alta tecnologia. As suas aplicações principais em alta tecnologia incluiem catálise, vidros, pós, magnetes, produtos fluorescentes, cerâmicos e lasers, importantes na conversão de energia solar, telecomunicações e etiquetas de segurança, bem como em cirurgia e imagem médica, e na indústria de defesa.

**SUMMARY**

The Rare Earths are a group of 17 elements, including the lanthanoid elements scandium and yttrium, which cover the 4f-block row of the Periodic Table. Their discovery has a complex history due to their chemical similarity. Their abundance in the Earths crust shows that they are not rare, but their main known deposits and world production are concentrated in China, making then strategic for the technology needs of the western nations. Although the light rare earths are more abundant than the heavier ones, the later have much more important applications, causing some of the later ones to be critical. The recycling of those elements is a solution that is starting to be implemented. Their electronic subshell containing 0 to 14 4f-electrons provides the similar chemical properties, dominated by the 3+ oxidation state. The basis of their coordination chemistry and catalytic effects is described, as well as their magnetic and luminescent properties, which are crucial to the manufacture of many high-technology contemporaneous products. The main applications of these elements in high technology include catalysts, glasses, powders, alloys, magnets, phosphors, ceramics and lasers, important in solar energy conversion, telecommunications and security tags, in medical surgery and imaging and in the defense industry.

[1] Departamento de Ciências da Vida, Universidade de Coimbra (DCV).
[2] Centro de Química de Coimbra – Instituto de Ciências Moleculares (CQC-ICM).

## 1. INTRODUCTION TO THE RARE EARTHS

Rare Earths (RE) are a group of 17 elements, including the 15 lanthanoid elements lanthanum (La) to lutetium (Lu), of which the 14 elements cerium (Ce) to Lu are the lanthanides, plus scandium (Sc) and yttrium (Y). The lanthanoid elements span the 4f-block row of the Periodic Table (Figure 1). They are chemically similar elements, but their varied physical properties are crucial to the manufacture of many high-technology contemporaneous products. The lanthanide atoms have a subshell containing 0 to 14 4f-electrons, which provide the elements with important magnetic and luminescent properties. [6]

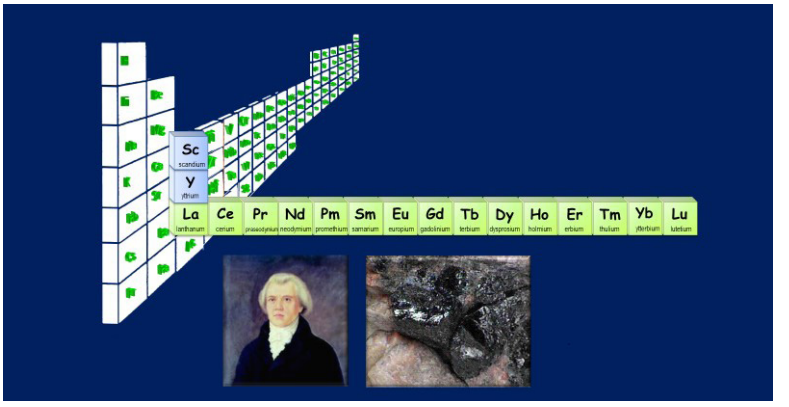


Figure 1.
Position of the rare-earth elements in the periodic table and their official IUPAC nomenclature, a portrait of Johan Gadolin, and a picture of the black stone of Ytterby. Adapted from ref. 19.

The history of the discovery of the RE elements is quite complex, full of conflicting and, often incorrect claims, due to their similar chemical properties. It started in 1887 when Carl Axel Arrhenius, a swedish army lieutenant and amateur mineralogist, found a black mineral in an old quarry near Ytterby, 30 km from Stockholm, and named it "ytterbite". Analysis of this heavy stone ("tungsten" in Swedish) by mineralogist B. R. Geijer confirmed that it was a new mineral, measured its density ($d$ = 4.2) and hypothesized that it may contain tungsten.[21] In 1894, Johan Gadolin, professor at the University of Abø, then in Sweden, but today known as Turku in Finland, published a report in in the Proceedings of the Royal Swedish Academy of Sciences, concluding to the presence of a new "earth", which he named "yttria". In 1797, A. G. Ekeberg confirmed Gadolin's analysis and proposed to rename the mineral gadolinite, with formula $Y_2FeBe_2SiO_{10}$. These events initiated a series of investigations by brilliant European scientists, which eventually led to the identification of 16 stable RE elements. It was shown that "yttria" contained the oxides of ten RE elements: yttrium (Y- Mosander, 1795), erbium (Er - Mosander, 1879), thulium (Tm - Cleve, 1879), scandium (Sc - Nilson, 1979), gadolinium (Gd - Galissard de Marignac, 1886), terbium (Tb - Mosander, 1886), dysprosium (Lecoq de Boisbaudran, 1886), holmium (Ho- Cleve, Soret and Delafontaine, 1886), ytterbium (Yb - Galissard de Marignac, 1907) and lutetium (Lu - Urbain and Welsbach, 1907) . From the mineral "ceria", the light RE elements cerium (Ce – Berzelius and Mosander, 1839), lanthanum (La- Mosander, 1841), praseodymium and neodymium (Pr, Nd – Welsbach, 1885), samarium (Sm, - Lecoq de Boisbaudran, 1901) and europium (Eu - Demarçay, 1901) were isolated. The last, radioactive RE (promethium- Pm) was synthesized in 1947 at the Oak Ridge National Laboratory, USA, by Marinsky, Glendenin and Coryell (Figure 2). [45, 56]

C.A. Arrhenius
**gadolinite**

B. R. Geijer
**gadolinite**

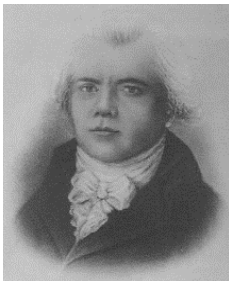

J. Gadolin
**Y**

A. G. Ekeberg
**(yttria)**

A. F. Cronstedt
**cerite**

J. J. Berzelius
**Ce**

W. Hisinger
**Ce**

M. H. Klaproth
**Ce**

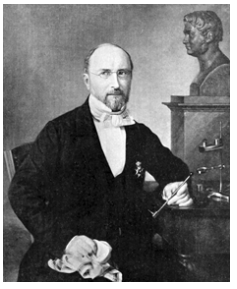

C. G. Mosander
**La, Er, Tb**

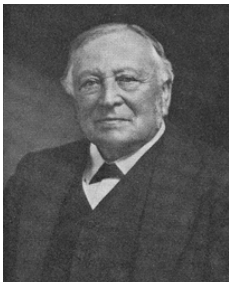

H. E. Roscoe
**Tb spectrum**

M. Delafontaine
**Ho**

J.-L- Soret
**Ho**

P. P. Cleve
**Ho, Tm**

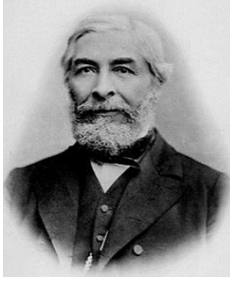

J. Galissart de Marignac
**Gd, Yb**

L. F. Nilson
**Sc**

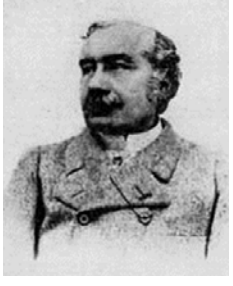

P. E. Lecocq
de Boibaudran
**Sm, Dy**

C. Auer von Welsbach
**Nd, Pr**

E. A. de Marçay
**Eu**

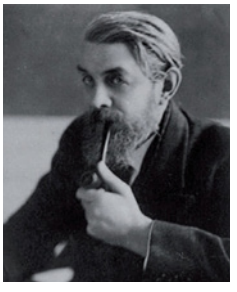

G. Urbain
**Lu**

J. A. Marinsky
**Pm**

Figure 2.
The twenty rare-earth pioneers (from Wikipedia).

The abundance of the rare earths in the Earth's crust (60 (Ce) - 0.5 (Lu) ppm) (Figure 3), makes the name of this family of elements misleading. The original minerals gadolinite ($RE_2FeBe_2Si_2O_{10}$) (35-50% RE) and cerite [$(Ca,Ce)_{10}(Fe^{III})(SiO_4)_6(OH,F)_5$)] (35-50% RE) are rare, but the elements are not, as over 270 minerals are known to contain these REs, often replacing $Ca^{2+}$ sites. The two commercially important mineral sources are monazite [(Ce, La, Nd, Th) $PO_4$] (50 – 75 % RE), and bastnäsite [$CeCO_3(OH, F)$] (65-70% RE). The lanthanide abundances in Figure 3 show an odd-even effect (Oddo-Harkins rule), with the element of odd atomic number (Z) being less abundant than the immediately adjacent elements of even Z values. The abundances of the even Z lanthanides decrease regularly from Ce to Yb, while those of the odd Z members decrease in parallel fashion from La to Lu. The basis for this rule is that elements with even Z are more abundant because their nuclei have more isotopes and the nucleons pair up with opposite spins. Ion-adsorption clays (0.05-0.2% RE), e.g. kaolinite, are the most important source of heavy RE elements (HREE).

The known world RE mineral reserves are estimated by the USA Geological Survey (USGS, January 2021) to be 116 million metric tons. They are located essentially in China (38%), Vietnam (19%), Brazil (18%) and Russia (10%), while the remaining are scattered in various countries such as India, Australia, USA, Canada, Malaysia, Sri Lanka, Thailand, and Poland. The USA was the most important single producing country for rare earth elements (REEs), from the Mountain Pass mine in southern California (Figure 4), which between 1965 and 1995 supplied most of the worldwide RE metals consumption. However, China developed its mines in the 1980s and 90s, such as the Bayan Obo mine (Inner Mongolia, Figure 4), which now is the world's largest REE mine both by recoverable reserves and production, accounting for more than 40% of the total known world REE reserves and nearly half of the global

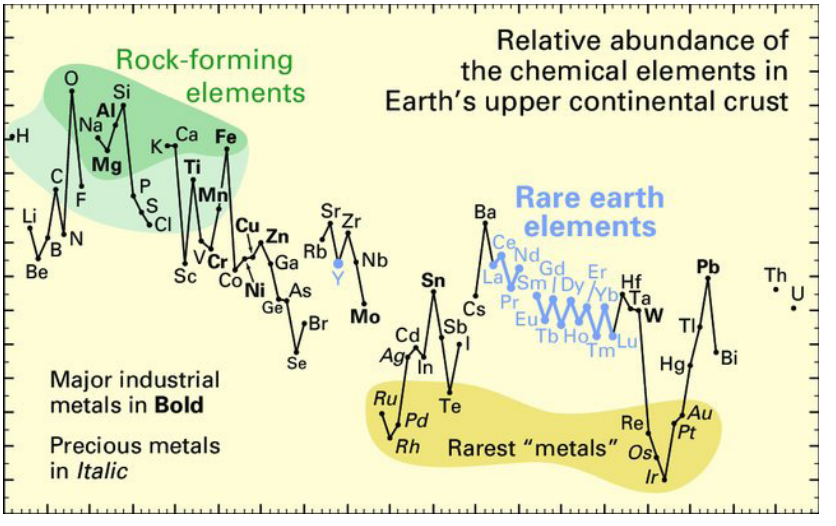


Figure 3.
Abundance (atom fraction) of the chemical elements in Earth's upper continental crust as a function of atomic number. Many of the elements are classified into (partially overlapping) categories: (1) rock-forming elements (major elements in green field and minor elements in light green field); (2) rare earth elements (lanthanides, La–Lu, and Y; labeled in blue); (3) major industrial metals (global production ≥ $3x10^7$ kg/year; labeled in bold); (4) precious metals (italic); and (5) the nine rarest "metals"- the six platinum group elements plus Au, Re, and Te (a metalloid). Reprinted from ref. 37.

RE production. This development gradually drove the Mountain Pass mine out of business, which closed in 2002 after a toxic waste spill. RRE production in China, was, in 2011, 96% of the overall production, which therefore completely controlled the market, setting up quotas for its customers. As RE substitutes available for several applications are generally less performing, the risky geopolitical situation evolved, so that several countries resumed or started mining operations and REE production. An example is the Mountain Pass mine, which was reopened in 2012 and in 2020 supplied 15.8% of the world's light RE (La, Ce, Nd, Eu) production from bastnäsite. The evolution of global production of RE oxides (REOs) by China, USA and other countries is shown in Figure 5. As a consequence of this variation in RRE production sources, the average price of REOs increased sharply from 15 US $/kg REO in 2008 to a maximum of 160 US $/kg REO in 2011 and decreased back to 18 US $/kg REO in 1016, while the world REO production stayed basically constant at 120 ktons/year in the same 2008-2016 period.

Figure 4.
Left: Mountain Pass mine (California; USA); right: Bayan Obo mine (Inner Mongolia, China). (from Wikipedia)

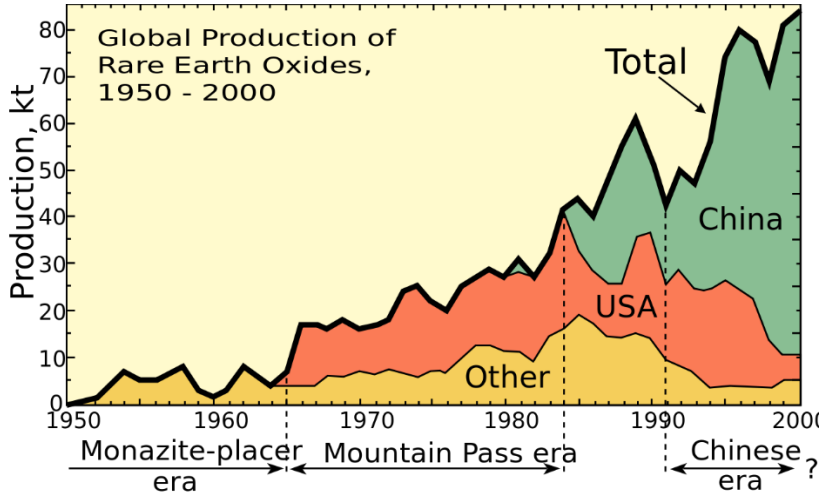


Figure 5.
The Mountain Pass mine dominated worldwide REE production from the 1960s to the 1980s, but China dominates world REE production (USGS). Reprinted from ref. 37.

The production of REEs, represented schematically in Figure 6, is a complex and polluting process, starting at deposit exploration, followed by mining and production of RE ore concentrates by benificiation, where the raw ore is physically processed to remove gangue minerals. This is followed by extraction of REEs from concentrates by acidic or alkaline chemical dissolution treatment to obtain a mixture of RE salts, and their separation and purification, for example by solvent extraction or ionic exchange and precipitation, obtaining the individual REOs, followed by refining to obtain the individual metals, for which there are many different methods, such as calcination. [30, 51]

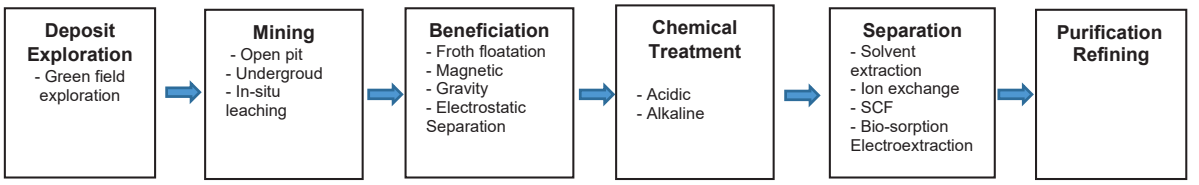


Figure 6.
Schematic of REE processing steps. Adapted from ref. 48

Recent increase in the demand for REEs, especially Dy and Tb used in the permanent magnet industry, is modifying the industrial approach to REE mineralogy and resources. [3,33] This is amplified by the REE supply restrictions outside of China and by the fact that REEs are never mined individually but always as mixtures with various compositions. However, although there are uses for all REEs, the most useful are often the less abundant. These compositions, however, do not necessarily correspond to the demand for individual REEs. Some elements are in surplus (La, Ce), as the major ores contain light REES, while others are in tight supply (or more utilized) and are classified as "critical.", which applies to any substance used in technology that is subject to supply risks, and for which there are no easy substitutes. An example is that a 400-600 kg magnet for a wind turbine, of composition $Fe_{14}Nd_2B$, contains 4-8% Dy (20-50 kg Dy) and at the Bayan Obo mine, for obtaining 1 kg Dy one needs to produce 500 kg Ce, while in Mountain pass, 1500 kg Ce are produced to obtain 1 kg Dy. This imbalance problem is difficult to solve, but the surplus REEs need to have new applications found. Although, as a whole, REEs are not "critical", some of them are, which include Y, Nd, Eu, Tb and Dy (Figure 7). [4] Exploration has now been extended worldwide to secure the supply of REEs, especially the heavier ones (HREEs, Gd–Lu), which are the most critical group of elements for future green technologies. (Figure 7). In recent years, various attempts have been made to produce HREEs from unconventional sources, such as peralkaline igneous rocks or deep-sea muds. [55] Besides finding new sources of "critical" RREs, strategies are needed to substitute, reduce utilization, reuse and recycle them. [3]

Although presently only less than 1% of REEs are recycled, the goal is to reach globally 10-20%, and the European Union has a potentiality of attaining > 50% REEs from recycling. For this aim, economical aspects and ease of dismantling RREs- containing devices have to be considered: scrap material at manufactures are easier to recycle, while end-of-life recycling is more difficult. Major recyclig plants are from Hitachi (Tokyo Eco Recycle Ltd) in Japan, recycling REEs from magnets in air-conditioners and dishwashers, Rhodia-Solvay recycling phosphors and lamps in France and Ames recycling Nd from magnets in the USA.

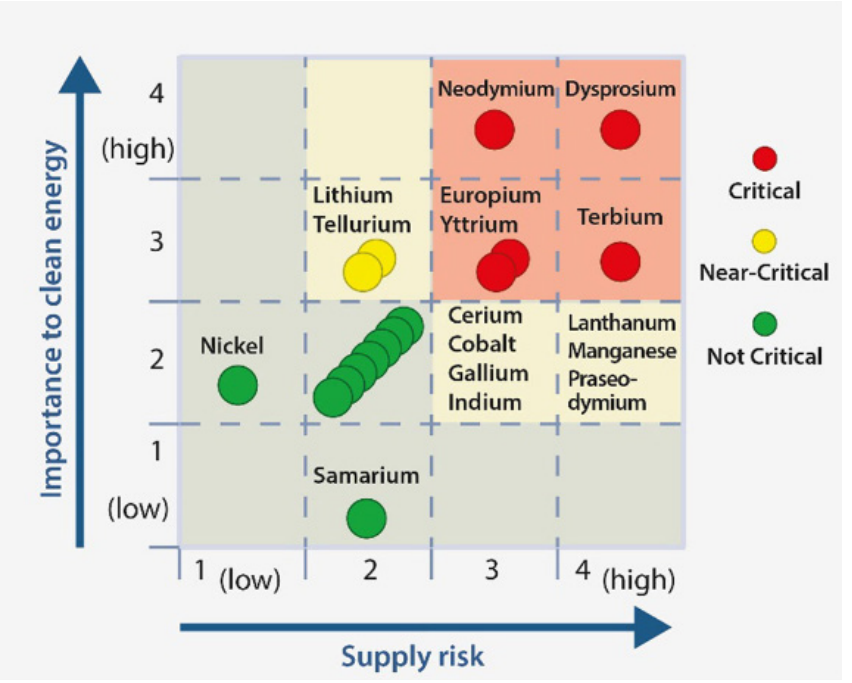


Figure 7.
DOE medium-term (2015–2025) criticality matrix, showing the five most critical rare-earth elements (Nd, Eu, Tb, Dy, and Y). Reproduced from ref. 4 with permission under the terms of the Creative Commons Attribution 4.0 International License (http://creativecommons.org/licenses/by/4.0/). Copyright 2018 Springer

## 2. BASIC PROPERTIES OF THE RARE EARTHS

The rare earth metals are gray to silvery and often malleable, with high melting and boiling points. The strong similarity in the properties of the lanthanide elements results, in part, from their common existence in the trivalent state ($Ln^{3+}$). This trivalency is due to the relative energies of the 4f, 5d, 6p and 6s electron orbitals (Figure 8) in the Z =57 – 71 range. While the ionization energies of the elemental atoms ($Ln^0$) to form the $Ln^+$ and $Ln^{2+}$ gaseous ions are quite constant along the lanthanide series, they show stronger variations for the $Ln^{2+} \rightarrow Ln^{3+}$ and $Ln^{2+} \rightarrow Ln^{3+}$ processes. These result from the electron configurations of the Ln along the series. $Ln^+$ and $Ln^{2+}$ are formed by ionization of the electrons in the 6s orbital. The third ionization to form $Ln^{3+}$ results, in most cases, from the removal of a 5d electron, because the 4f orbitals are lower in energy than the 6s and 5d orbitals. Thus, the $Ln^{3+}$, with configurations $[Xe]4f^n$ (n = 0 -14) for La-Lu, differ in a regular pattern of successive electron occupation of the 4f orbitals as Z increases. These 4f orbitals have less radial extention and do not participate in covalent bonding to an extent comparable to the d orbitals in transition metal ions.

The inner character of the 4f electrons in $Ln^{3+}$ cations is illustrated in Figure 9, which shows for $Nd^{3+}$, that the radial distributions of most of the 4f orbitals are much less extended than the 5s and 5p orbitals. Therefore, the chemical, magnetic and spectroscopic properties of the $Ln^{3+}$ ions and their compounds are fully dependent of their 4f orbitals. [32]

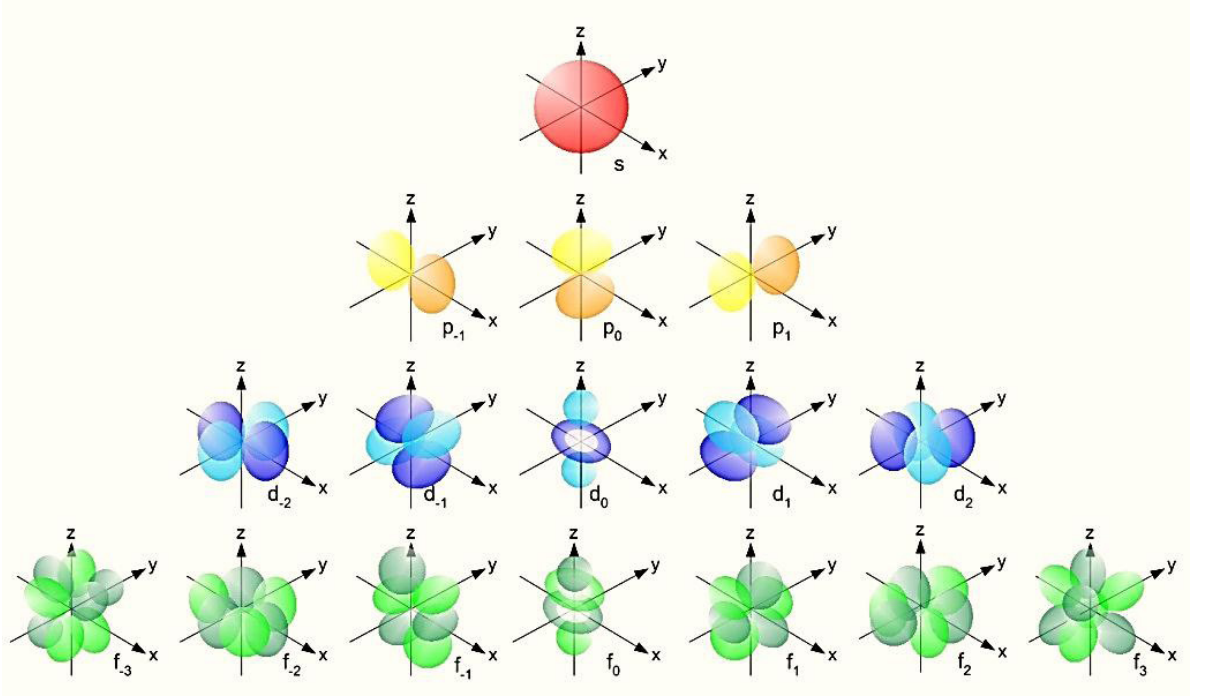


Figure 8.
Schematic representation of the shapes of the s, p, d and f orbitals. Reproduced from https://energywavetheory.com/atoms/orbital-shapes/.

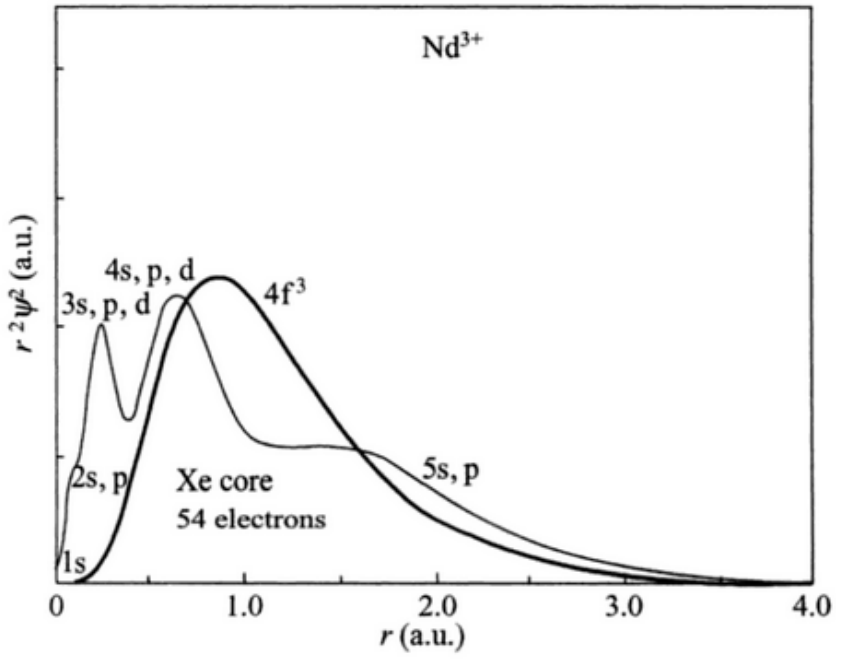


Figure 9.
Radial wave function r22 as a function of r in atomic units for 4f3 electrons of Nd3+ in comparison with the charge distribution of its core (Xe) configurations. Reprinted from ref. 32, open access. Copyright 2005 Springer.

The $Ln^{3+}$ cations behave as Lewis acids, establishing ionic coordination bonds with Lewis bases, such as fluoride and oxygen anions. Their ionic radii (r) in aqueous solution decrease along the series as Z increases (lanthanide contraction by $\Delta r = 0.255$ Å) from 1.250 Å ($La^{3+}$) to 0.995 Å ($Lu^{3+}$) (Figure 10) [17]. These values are slightly different from crystal ionic radii listed by Shannon for 9-fold $Ln^{3+}$ coordination (1.216 Å ($La^{3+}$) to 1.032 Å ($Lu^{3+}$), $\Delta r = 0.184$ Å) [47].

The ionic radii increase with the coordination number for all $Ln^{3+}$.Their reduction potentials $E_{(III/0)}$ are quite negative and are almost constant along the series (La = -2.37 V to Lu = -2.30 V in acidic conditions). [14] The coordination number (CN) of the aqueous $Ln^{3+}$ ions is 9 for La-Sm, a 9/8 equilibrium for Eu-Ho and 8 for Er-Lu. The strong ionic nature of the coordination bonds results in coordination geometries that reflect a balance of electrostatic and steric demands of the ligand, as well as solvation effects (Figure 12). Examples are square antiprimatic (SAP) geometry for CN = 8 (eg. $[Lu(DOTA)]^-$ (DOTA = 1,4,7,10-tetraazacyclododecane-1,4,7,10-tetraacetic acid) and mono-capped SAP geometry for CN = 9 (eg. $[Gd(DOTA)(H_2O)]^-$).

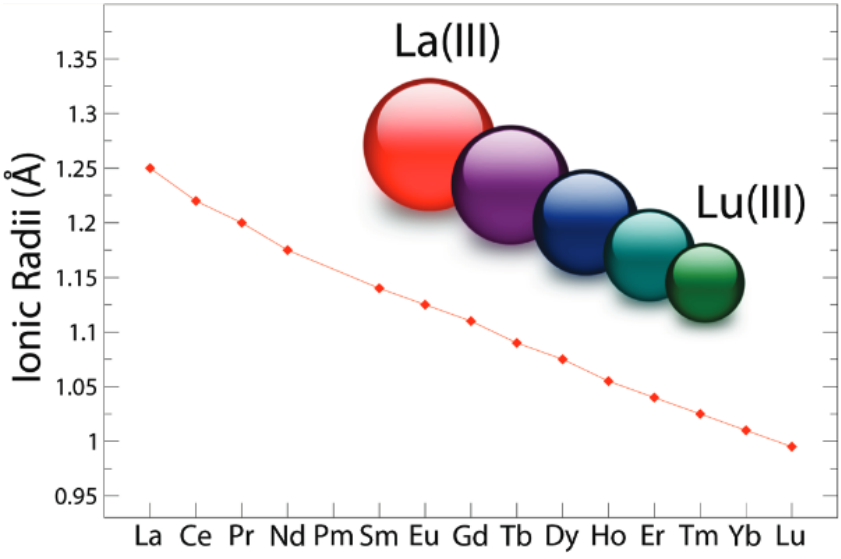


Figure 10.
Ionic radii (Å) of Ln3+ ions in aqueous solution obtained from a very accurate experimental determination of the ion- water distances obtained from extended X-ray absorption fine structure (EXAFS) data. Reprinted from ref. 17 with permission. Copyright 2011, American Chemical Society.

The thermodynamic stability constants of lanthanide complexes increase sharply with the number of chelates formed in the complexes, which reflects dominant entropic effects [14] (Figure 11). [59,61] The $[Ln(acetate)_4]^-$ complexes, with one chelate per ligand, has stability constants (log $K_1$) of 2.0 – 2.5 along the series, whereas the log $K_1$ values of the $[Ln(EDTA)(H_2O)_3]^-$ (EDTA = ethylenediammine-tetraacetate), with five chelates per ligand) increases from 15.2 (La) to 19.8 (Lu) and $[Ln(DTPA)(H_2O)]^-$ (DTPA = diethylenetriaminepentaacetic acid), with seven chelates per ligand, increases from 19.8 (La) to 22.5 (Lu).

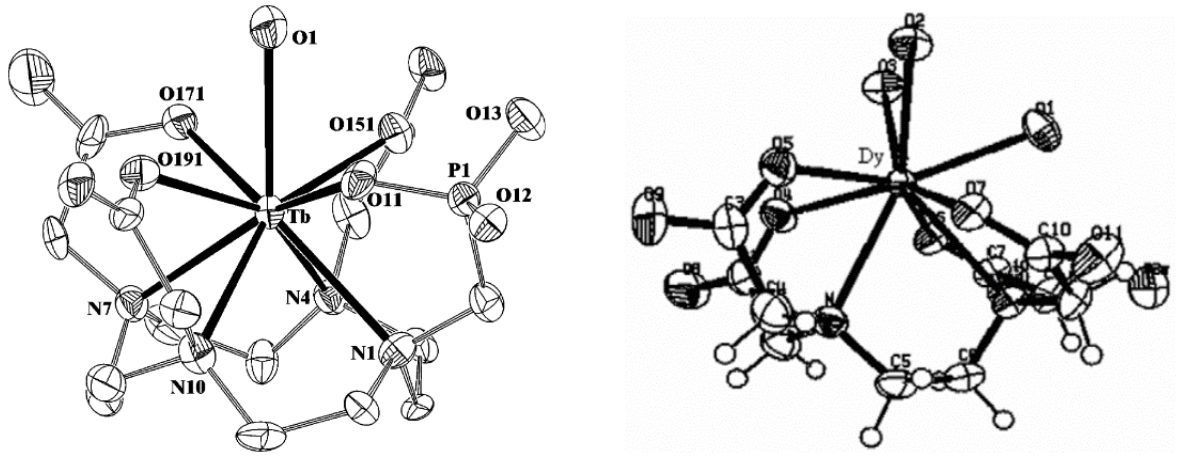


[Tb(III)-HDO3AP)($H_2O$)]$^-$
7 chelates

[Dy(III)-EDTA($H_2O$)$_3$]$^-$
5 chelates

Figure 11.
X ray crystal structures of [Tb(III)-HDO3AP)($H_2O$)]$^-$(HDO3AP = 1,4,7,10-tetraazacyclododecane-4,7,10-tris(carboxymethyl)-1 methylphosphonic acid) and of [Dy(III)-EDTA($H_2O$)$_3$]$^-$. Reprinted from ref. 59 (right) and ref. 61 (left) with permission. Copyright 2005, American Chemical Society.

The $Ln^{3+}$ cations are paramagnetic, except $La^{3+}$ ($4f^0$) and $Lu^{3+}$($4f^{14}$), which are diamagnetic. The 3d transition metal cations, where the spin moment alone determines their magnetic moments, due to the quenching of the orbital angular momentum contribution by interactions with the field of the surrounding anions, dipoles, etc., have a maximum paramagnetism coinciding with the maximum number of unpaired electrons in the 3d orbitals. However, the magnetic moments of the $Ln^{3+}$ show two maxima, neither of which is associated with the $4f^7$ configuration of maximum multiplicity. This binodal variation can be derived considering that their magnetic moments are calculated by including both the orbital and spin contributions. [31] The pink circles in Figure 12 represent the effective magnetic moments ($\mu_{eff}$) in Bohr magnetons of the $Ln^{3+}$, calculated from the Landé equation for their magnetic susceptibility $\chi_m$ (1)

$$\chi_m = \frac{N g_J^2 \beta^2 J(J+1)}{3kT} \qquad (1)$$

using the relationship of $\chi_m$ and $\mu_{eff}$ given by equations (2) and (3):

$$\mu_{eff} = \sqrt{\frac{3kT\chi_m}{N\beta^2}} \qquad (2) \qquad \mu_{eff} = g_J\beta\sqrt{J(J+1)} \qquad (3)$$

where $N$ is Avogadro's number, $g_J$ is the Landé splitting factor, $\beta$ is the Bohr magneton, $J$, $L$ and $S$ are the total, orbital and spin quantum numbers of the $Ln^{3+}$ ($J = L+S$, Russell-Saunders coupling), $k$ is Boltzmann's constant and $T$ the temperature in Kelvin. The experimental values in Figure 12 agree well with the calculated values using Landé equation, except for $Sm^{3+}$ and $Eu^{3+}$. At room temperature, these ions have small populations of the lowest lying excited electronic states (excited levels within $kT$ of the ground level). Inclusion of the contributions from population of these excited levels, using Van Vleck's equation (blue squares in Figure 12) gives much better results, in good agreement with the experiments. [31]

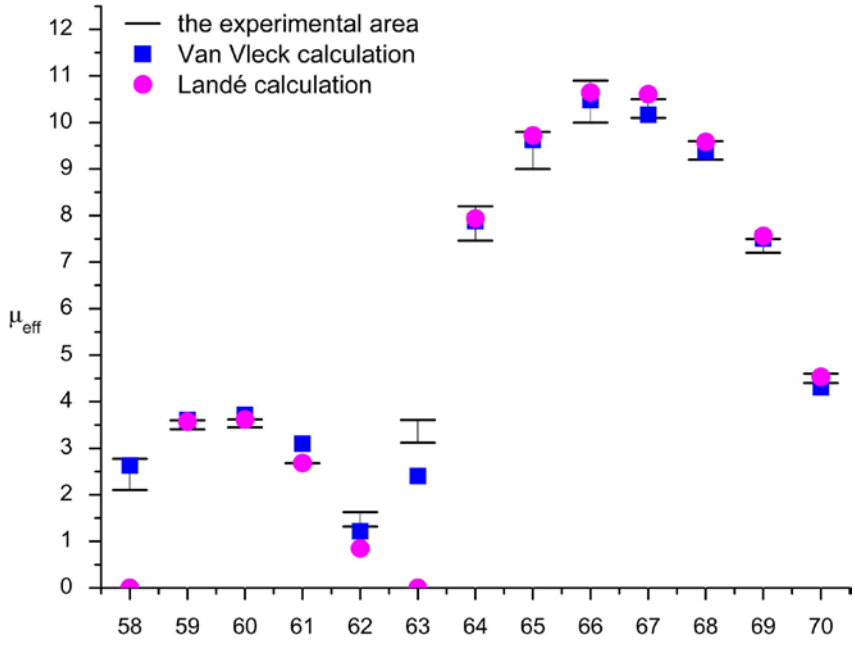


Figure 12.
Effective magnetic moments ($\mu_{eff}$, in Bohr magnetons) of the $Ln^{3+}$ ions *vs*. their atomic numbers (Z) at room temperature (Ce, Z= 58; Eu, Z = 63, Yb, Z = 70). Reprinted from ref. 31 with permission. Copyright 2013 Elsevier.

Due to their usually large magnetic moments and large magnetic anisotropy, $Ln^{3+}$ complexes can form single molecule magnets (SMM). A single-molecule magnet is a metal-organic compound which can be magnetized using a magnetic field, yet still remains magnetized once the magnetic field is removed. It has a superparamagnetic behaviour below a certain blocking temperature at the molecular scale. In this temperature range, a SMM exhibits magnetic hysteresis of purely molecular origin. In contrast to conventional bulk magnets and molecule-based magnets, collective long-range magnetic ordering of magnetic moments is not necessary. SMM could revolutionize the fabrication technology of computer memory chips. [35] An example of SMMs is a series of phthalocyanine double-decker complexes, $[Pc_2Ln]^-$,$TBA^+$ (Ln =Tb, Dy, Ho, Er, Tm, or Yb; Pc = dianion of phthalocyanine; $TBA^+ = N(C_4H_9)^{4+}$) (Figure 13). [26]

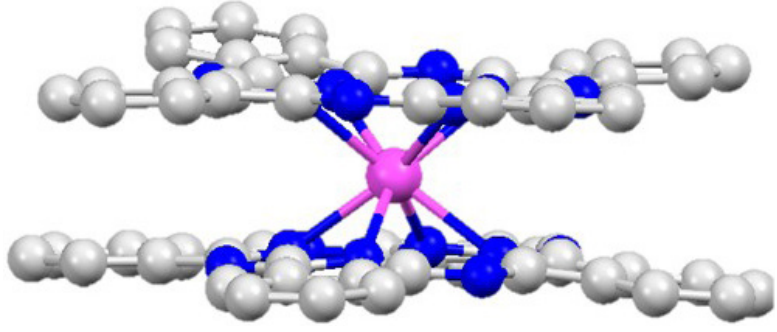

Figure 13.
Phthalocyanine double-decker complexes, $[Pc_2Ln]^-$ (Ln =Tb, Dy, Ho, Er, Tm, or Yb; Pc = dianion of phthalocyanine) are promising SMMs. Reprinted from ref. 26 with permission. Copyright 2003, American Chemical Society.

$Ln^{3+}$ ions and complexes radiate luminescent light when stimulated by an energy source, like a laser or lamp, of proper wavelength, which excites their 4f electrons from a ground electronic state into an excited state, which, after a short time, fall back into its ground state, emitting light. However, these electronic states are not pure and contain contributions from vibrational energy of the motion of the nuclei concerned. This results in the subdivision of each electronic level into associated vibronic levels. Thus, after the electronic excitation, two fast processes bring the 4f electrons back to lower states: a) vibrational relaxation (VR,$10^{-12}$ – $10^{-14}$ s), where the excited $Ln^{3+}$ in a complex loses vibrational energy by collisions with the solvent molecules, or by exchange with the vibrational motions of a solid matrix where it is included; b) internal conversion (IC, $10^{-12}$ s), where the molecule is transferred to a highly excited vibrational level of the ground state. Then, the lowest vibrational level of the ground state can be reached by vibrational relaxation. Sometimes, the IC process involves a change in the spin of the transferred electron, which reaches states having a higher spin quantum number (S) than both the original ground and excited states. This IC process is slower ($10^{-8}$ s) and is called intersystem crossing (ISC). All these processes do not result in the emission of light and are known as non-radiative processes. Radiative transitions result from f → f electron transitions on the $4f^n$ shell of the $[Xe]4f^n$ (n = 0, 14) configurations. These can lead to fluorescence (which takes $10^{-6}$ – $10^{-12}$ s) or phosphorescence (taking $10^{-6}$ to several seconds), corresponding to the emission of light associated with the transitions from the excited states. Phosphorescence is much slower because it involves a change of spin. [7, 18, 24] The corresponding luminescence bands occur in the UV (Gd), Vis (Pr, Sm, Eu, Tb, Dy), and near infrared (NIR) (Nd, Ho, Er, Tm, Yb) emission regions by fluorescence (ΔS = 0), phosphorescence (ΔS > 0), or both (Figure 14). [15]

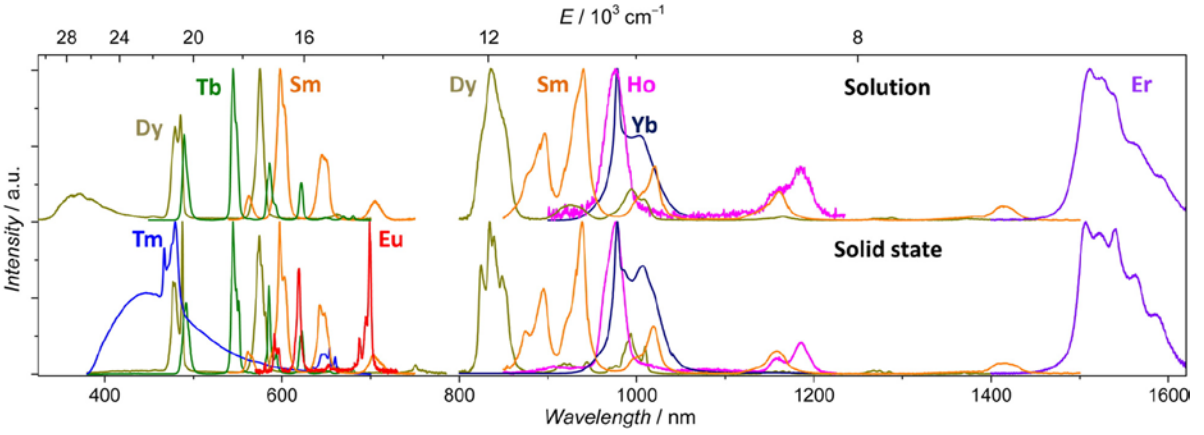


Figure 14.
Normalized emission spectra of luminescent lanthanide complexes in CD3OD solution and in the solid state under ligand excitation at 320–350 nm at room temperature. Reprinted from ref. 15 with permission. Copyright © 2016, American Chemical Society.

Due to shielding by the filled 5s and 5p orbitals, the 4f orbitals participate in chemical bonding to the ligand atoms only to a very small degree. As a consequence, their emission bands are sharp, with wavelengths almost unaffected by the chemical environment, and with small Stokes shifts. The f → f transitions are formally forbidden by the spin selection rule. They are either magnetic dipole (MD) transitions, which are allowed by the parity (or Laporte) selection rule, or electric dipole (ED) transitions, forbidden by that rule. However, those rules are relaxed by several mechanisms, such as coupling of the electronic states

with vibrational states of the ligand, which changes temporarily the geometry around the metal ion, and thus, its symmetry. In practice, the bands in the absorption spectra are usually quite weak, and the observed luminescence lifetimes are much longer (ms–µs) than those of the short-lived (ns) autofluorescence and scattering from the biological background, which allows their suppression by time resolved detection (TRD) of luminescence. The intensity of some of the transitions is quite sensitive to the nature of the $Ln^{3+}$ ion environment and are called "hypersensitive", e.g., the Eu ($^5D_0 \rightarrow {}^7F_2$) transition. [7, 18, 24]

As the bands in the absorption spectrum are usually weak, direct excitation of the $Ln^{3+}$ rarely yields highly luminescent compounds. The use of intense light sources such as lasers to directly populate the excited states of the $Ln^{3+}$ is not practical for biological systems. Thus, indirect excitation (called sensitization or antenna effect) [61] is required to provide luminescence strong enough to allow biological imaging applications. Figure. 15 shows a simplified diagram of this complex process. [7, 11, 18, 24] First, light is absorbed to yield the short-lived singlet excited state of the light-harvesting antenna ($S_0 \rightarrow S_1$), an organic chromophore attached to the immediate environment of the $Ln^{3+}$. The antenna can then undergo intersystem crossing (ISC) to the longer-lived lowest triplet excited state $T_1$ ($S_1 \rightarrow T_1$). Sensitization results from the population of the lowest (or several) excited state(s) of the $Ln^{3+}$ through energy transfer (ET) from the $T_1$ state of the antenna. ET can also occur from the $S_1$ state, but the $T_1$ state, with longer lifetime, is the main donor state.

Finally, the metal ion emits photons due to electronic transitions from the excited state(s) to the ground state(s) of the $Ln^{3+}$ ($^5D_J \rightarrow {}^7F_J$) in $Eu^{3+}$ or $Tb^{3+}$), characterized by a series of line-like bands covering the UV, VIS or near-infrared (NIR) wavelengths provided by the large Stokes shifts (Figure 14) [15, 42], which allow multiplex detection. On the basis of this mechanism, a typical $Ln^{3+}$ -based optical probe consists of three major components, a luminescent metal center, a protective chelate, and a sensitizing antenna linked to it (Figure 15) [24].

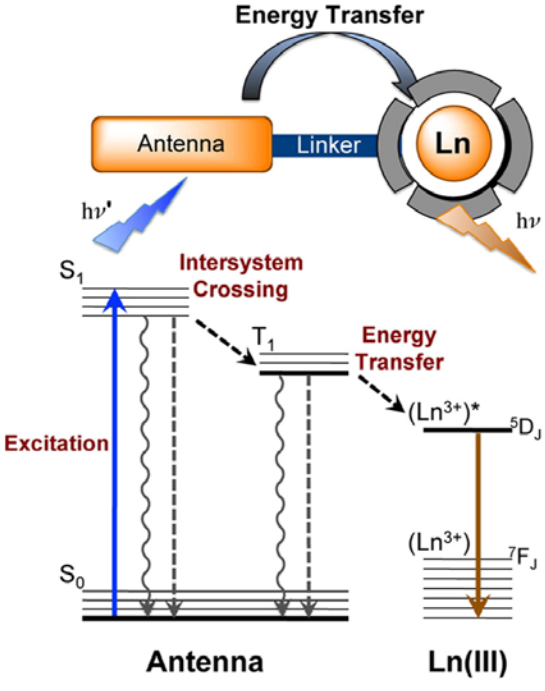


Figure 15.
Diagram illustrating the antenna effect, e.g., for $Eu^{3+}$ and $Tb^{3+}$ complexes. Schematically, emissive $Ln^{3+}$ complexes consist of a metal center bound by a chelate attached to a sensitizer or antenna. The chelate protects the lanthanide from quenching by oscillators like O–H of water. The antenna collects energy through efficient absorption to the singlet excited state $S_1$. After intersystem crossing to the triplet state $T_1$, the antenna transfers energy to the excited $^5D_J$ state of the $Ln^{3+}$ ion. Luminescent emission from the $Ln^{3+}$ ion results from the radiative transition of electrons from the excited $^5D_J$ state to the $^7F_J$ states. Reprinted from ref. 24 with permission. Copyright 2014, American Chemical Society.

### 3. Rare Earth applications in Science and Technology

Since their discovery, REs initially did not find practical applications, except for strongly stimulating general science and technology, particularly spectroscopy. This totally changed when the Austrian entrepreneur Carl Auer von Welsbach, the discoverer of Pr and Nd (Figure 2), filed two patents, the first one (1901) describing an incandescent gas mantle made up of thorium oxide doped with 1% of tetravalent cerium oxide, and the second one (1903) describing the production of flint stones from "Mischmetall", an alloy of 30% iron and 70% La, Ce, Nd and Sm. However, in recent decades, REs became vital to the development of many advanced materials and technologies. Sometimes RE applications do not involve large quantities, as several materials owe their special properties to doping of REs at low concentration, e.g. optical fibres with 35 ppm of $Er_2O_3$ doped in silica. The annual consumption in 2011 is estimated to 130000 metric tons of equivalent rare-earth oxides with a total worth of 15000 million US dollars. The three major applications, catalysts, alloys and magnets, correspond to about 60% of this consumption (Figure 16). Three others, polishing powders, optical glasses and light-converting phosphors account for about 30%, while ceramics (6%) and others (6%) complete the consumption distribution.

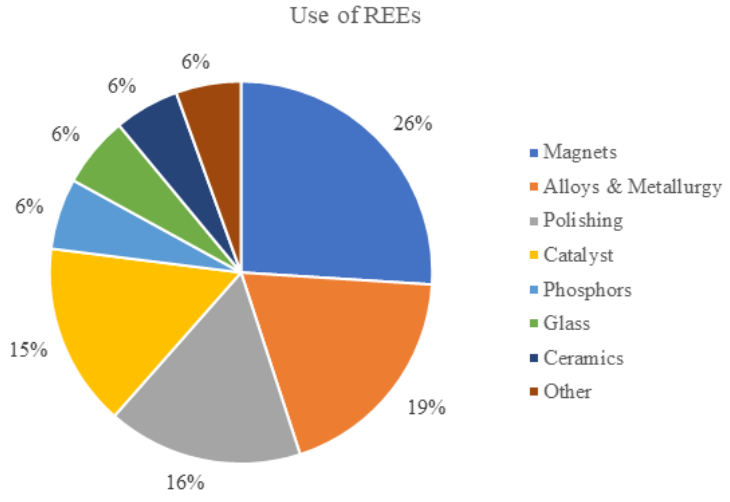


Figure 16.
Weight percentages of rare earths used in their main industrial applications in 2009 (data from the U.S.A. Geological Survey)

Cerium dioxide ($CeO_2$) materials are extensively used as industrial catalysts, such as catalysts for automobile exhaust, petroleum cracking and organic chemical synthesis. It has been used as a support, promoter, and active species as catalysts in various reactions, due to its cubic fluorite structure with oxygen vacancy defects ($CeO_{2-x}$), which has the capability to modulate $Ce^{4+}/Ce^{3+}$ redox couple depending on oxygen availability, shifting between $CeO_2$ and $Ce_2O_3$ under oxidizing and reducing conditions, respectively, using the equation $8\ CeO_2 \Leftrightarrow 4\ CeO_2 + 2\ Ce_2O_3 + V + O_2$ (V = vacancy). This property, known as oxygen storage capacity, is at the heart of its first important application, the control of automotive exhausts by selective catalytic transformation of $NO_x$, hydrocarbons and CO to $N_2$, $H_2O$ and $CO_2$ in the so-called three-way catalysis (Figure 17) [37]. From 1980 onwards, the use of $CeO_2$ has strongly expanded to affect several processes in the broad area of catalysis for energy and environment, such as self-cleaning

ovens coated with $CeO_2$, water purification by adsorbing impurities by $CeO_2$ nanoparticles, $CeO_2$ in solar-induced synthesis of kerosene, fluid catalytic oil cracking by La, Ce -containing zeolites, and $Nd^{3+}$-versetate as organic catalyst of butadiene polymerization to 98% cis-polybutadiene used in tyres. [2]

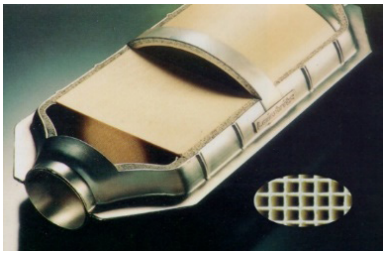

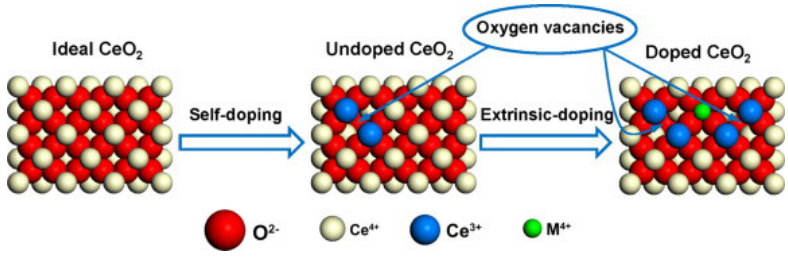


Figure 17.
Creation of oxygen vacancies in $CeO_2$ by self-doping and extrinsic doping (left); automobile three-way catalyst for exhaust gases, EOLYS®, from Rhodia, reduces soot emission of Diesel engines by 99.9 %. Reprinted from ref.37. Copyright 2018 Elsevier (left); adapted from personal gift of Bünzli, J.-C. G. (right)

$CeO_2$-based powders are used to polish hard materials like optical glasses for screens, windows, mirrors and lenses used for spectacles, telescopes (like the Hubble telescope) and lasers. $La^{3+}$ and $Er^{3+}$ are crucial for making the infrared-absorbing glass in night vision goggles and cameras.

Lasers containing $Nd^{3+}$, $Ho^{3+}$, $Er^{3+}$ or $Yb^{3+}$, have many applications. The Nd:YAG (neodymium-doped yttrium aluminum garnet; $Nd:Y_3Al_5O_{12}$) laser, working at the 1064 nm wavelength, contains a crystal that is used as a lasing medium for solid-state lasers. It is used in medicine, such as ophthalmology for cataract surgery and acute angle-closure glaucoma, laser-induced thermotherapy to treat benign prostatic hyperplasia, cancer surgery to remove skin cancers, reduce benign thyroid nodules, and to destroy primary and secondary malignant liver lesions. They are also used in cosmetic medicine for laser hair removal and the treatment of minor vascular defects such as spider veins on the face and legs, and in dentistry for the removal of dental caries as an alternative to drill therapy. The Er-YAG laser beams (2940 nm wavelength) are a good option for minimally invasive surgeries because they are readily absorbed by water in flesh and thus won't slice too deep. High power lasers ($Yb^{3+}$ : YAG, emission at 1030 nm) are used in the manufacturing industry, such as metal cutting and laser peening in gas-fired turbine engines for both aerospace and power generation to increase strength and improve resistance to damage and metal fatigue. In the area of nuclear fusion, ignition has been recently reported at the National Ignition Facility, Lawrence Livermore National Laboratory, California, USA, using 500 TW lasers. Military applications of lasers have increased in the last years. Low energy lasers (< 1 kW power) are used in weapon simulation systems for training, for jamming the sensors in communication systems, or in anti-personal mode against the human eye. Medium energy lasers (10 kW - 100 kW power) are used for the destruction of optical or optoelectronic devices on the ground or space-based targets. High-Energy Lasers (HEL) (>100 kW power) are used for anti-aircraft or anti-missile systems. Lasers are also used in scientific research, such as flow visualization techniques in fluid dynamics, to build optical tweezers for biological applications, laser pumping, analysis of elements in the periodic table, and several types of spectroscopy, such as cavity ring-down spectroscopy (CRDS) and laser-induced breakdown spectroscopy (LIBS) [46, 60]

REs in ceramics include $BaTiO_4$: Nd additives for electronics in supercapacitors, microwave filters and oxygen sensors, electric motors with magnets containing Nd and Dy, rare earth ceramic oxides in coatings for corrosion protection of conductive power cables and high temperature (above the boiling point of liquid nitrogen, 77 K) superconducting ceramic materials for magnets. Typical materials include Sm-Co ceramics, LaOMX (M = Mn, Fe, Co, Ni; X = P, As) and YBCO ($YBa_2Cu_3O_{7-\delta}$), this one with a threshold temperature of around 92K, discovered by J. Georg Bednorz and K. Alex Müller (Nobel Prize of Physics in 1987), which was the first superconducting material at temperatures above that of liquid nitrogen, much cheaper and easier to handle than liquid He.[12] The discovery of these ceramic superconductors has changed superconductivity from an interesting curiosity to a useable technology, with particular applications in Magnetic Levitation (MagLev) trains in China and Japan, in the medical field as superconducting magnets in MRI scanners, in NMR and mass spectrometers, and in particle accelerators such as the large Hadron Collider.

The first alloy containing REs makes flint stones from "Mischmetall", an alloy of 30% iron and 70% La, Ce, Nd and Sm. More recent examples are magnetostrictive alloys for transducers in sonars, which change their shape under the influence of an external magnetic field, thus converting the energy in a magnetic field into mechanical energy. The cause of magnetostriction change in the length of materials is the result of the rotation of small magnetic domains. An example of such magnetostrictive materials is the $Tb_{0.3}Dy_{0.7}Fe_{1.92}$ alloy, known as Terfenol-D.[40] Other examples are a) cast pistons with added REs; b) AlMgLi-Sc alloys in military and civilian aircraft to improve fuel economy, manoeuvrability and range, which have also been used in the aerospace, automotive, energy (for solid oxide fuel cells), and 3D printing industries; c) nickel-lanthanide hydride (NiLnH) batteries, with Ni associated with the positive electrode and the negative–hydrogen storage electrode containing several REEs such as La and Ce, as part of the negative electrode od rechargeable batteries in electric and hybrid vehicles [34]; Yb atomic clocks, with an accuracy of $1{:}2\times10^{-18}$ 10 μK, which rely on about 10,000 Yb atoms cooled to 10 μK and trapped in an optical lattice of a series of pancake-shaped wells made of laser light. Another laser that "ticks" 518 trillion times per second provokes a transition between two energy levels in the atoms.

In the energy industry, Eu and Gd are used in making control rods in nuclear reactors. REEs agricultural fertilizers and feed additives have originated in China over the past several decades with the objective of increasing crop productivity and improving livestock yield (e.g., egg production or piglet growth). However, outside China, REE agricultural or zootechnical uses are not currently practiced. [57]

REEs most outstanding capabilities lie in their magnetism and luminescence and consequently their main industrial applications are in magnets, and luminescent devices like phosphors, generating light of different colours. REE-based magnets allowed their miniaturization while keeping their strength. SmCo ($SmCo_5$) magnets, developed in the 1960s, were the first popular REE magnets. Though slightly weaker than NdFeB magnets, they have have superior heat and corrosion resistance, so they were used in high-speed motors, generators, head-phones, turbomachinery, speed sensors in cars and airplanes, benchtop NMR spectrometers, and in the moving parts of some heat-seeking missiles. SmCo magnets also form the heart of most traveling-wave tubes, which boost signals from radar systems and communications satellites. Some of these tubes are transmitting data from the Voyager 1 spacecraft, currently the most distant human-made object (over 23 billion km away). Stronger and reliable NdFeB ($Fe_{14}Nd_2B$) permanent magnets support green energy production technologies in tidal power generation turbines

and wind turbines (650 Kg Nd), even offshore, to replace gearboxes, which boosts efficiency and decreases maintenance. Various car and bicycle parts, like motors, drivetrains, power steering and many other components of electric vehicles contain low Dy-content NdFeB magnets to increase their heat stability (Figure 18). Tesla's use of these in its farthest-ranging Model 3 vehicles has sparked supply chain worries. In conclusion, offshore wind turbines and hybrid/electric vehicles are two of the many applications that rely on rare-earth permanent magnets (REPM) to function. Although REPM have the high performance required, they contain significant amounts of Nd and Dy, whose supply is classed as being "critical" (see section 1). [49]

The development of Ln-based single-molecule magnets (SMMs) is very useful for high-speed computers and high-density magnetic storage devices (e.g. hard-disk drives). They exhibit the same properties as ferromagnetic substances and therefore each molecule may be used to store one bit of information (see Figure 14). Magnetic refrigerators rely on the magnetocaloric effect (MCE, also known as adiabatic demagnetization) which was discovered in iron by Warburg in 1881. This is an environmentally advantageous alternative to common cooling and refrigeration, which is based on compression/expansion cycles, which rely on and consume a large amount of chemical gases detrimental to the environment, more particularly to the ozone layer. MCE is the adiabatic temperature change ($\Delta T_{ad}$) occurring upon cooling or heating magnetic materials and is used to reach ultralow temperatures, near 0 K. It is intrinsic to any magnetic material and is due to the coupling of the magnetic sub-lattice with the magnetic field, which influences the magnetic part of the entropy. Among the many alloys and intermetallic compounds that have been tested, Gd, $Gd_5Si_4$ and specially a series of $Gd_5(Si_xGe_{1-x})_4$ ($0 < x < 0.5$) alloys displayed a large MCE. [9]

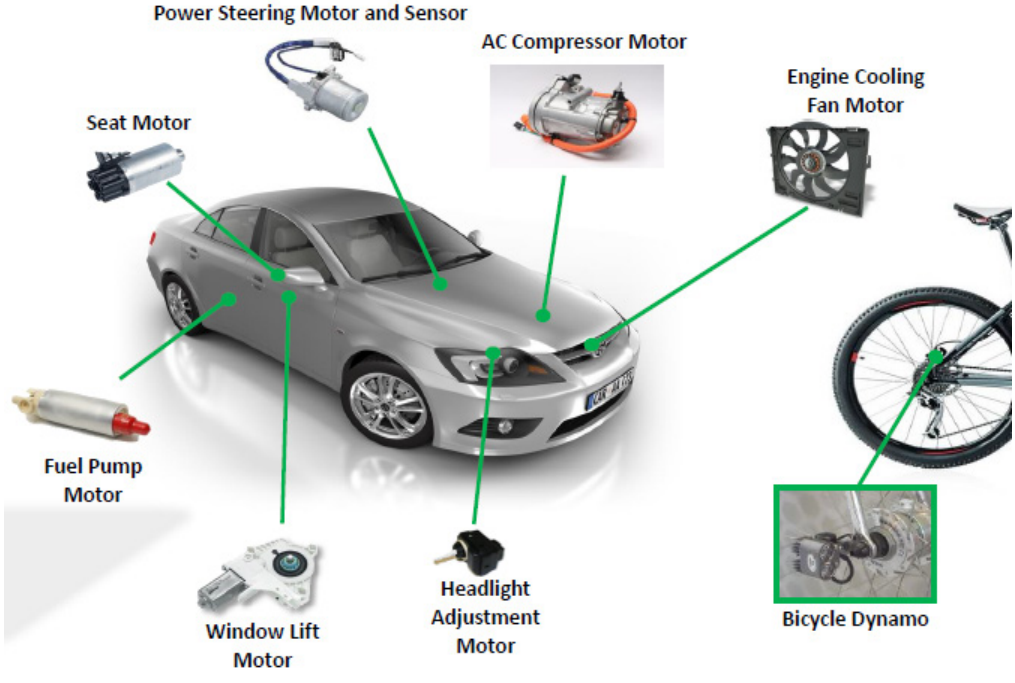


Figure 18.
Low Dy-content NdFeB ($Fe_{14}Nd_2B$) magnets in cars and bicycles. Adapted from personal gift of Bünzli, J.-C. G.

Stable $Gd^{3+}$ complexes are commonly used as contrast agents (CAs) in medical Magnetic Resonance Imaging (MRI). MRI was introduced in the 1980s and is based on Nuclear Magnetic Resonance (NMR) principles. There has been a trend toward clinical MRI equipment operating at higher magnetic field strengths ($B_0$), which is beneficial for higher contrast-to-noise ratios and better spatial resolution. At present, medical diagnostic MRI is typically performed at $B_0$ = 0.5–3 T, whereas research machines exist that operate at $B_0$ up to 11 T. Compared to other imaging techniques, it has tremendous advantages, including high spatial and temporal resolution, deep tissue penetration, and lack of ionizing radiation. The contrast in the images is generated by differences in intensities of $^1H$ NMR resonances, most frequently of water protons. Parameters including their local $^1H$ concentrations, longitudinal ($R_1 = 1/T_1$) and transverse ($R_2 = 1/T_2$) relaxation rates, and diffusion govern these intensities. Soon after the introduction of MRI, it became apparent that administration of contrast agents (CAs) may improve the quality and the information content of the images considerably [13]. Nowadays, about 40% of the MRI exams carried worldwide (approximately 30 million every year in the USA) use the administration of a CA. Usually, these agents contain strongly paramagnetic $Ln^{3+}$ ions, mainly $Gd^{3+}$ but also $Dy^{3+}$ and $Ho^{3+}$. These metal ions contain unpaired electrons that produce oscillating magnetic fields, which enhance the relaxation rates of protons in their proximity. The free metal ions are toxic, and therefore, their presence *in vivo* in a free form must be avoided. In the currently applied $Gd^{3+}$ based CAs, this can be achieved by encapsulation of the metal ion by a strong chelating ligand, such as linear or macrocyclic polyaminocarboxylates (Figure 19). The CAs are employed to differentiate between regions of interest that are histologically distinct, but magnetically similar. CAs increasing the $R_1$ values of water protons significantly more than their $R_2$ values give rise to bright spots in $T_1$-weighted MRI images and are called positive or $T_1$ CAs (Figure 20). Most of the presently applied Gd-based CAs belong to this class. $T_2$ or negative CAs increase the $R_2$ values of water protons significantly more than their $R_1$ values and result in dark spots in $T_2$ -weighted images. The main Ln-based representatives of this type are $Dy^{3+}$ and $Ho^{3+}$ chelates and nanoparticles.

Many types of Gd-based MRI CAs have been developed according to their biodistribution: extracellular, intravascular, hepatobiliary, cell or tissue targeted, responsive, etc., and some of these have reached the clinical use. [22, 24, 58]

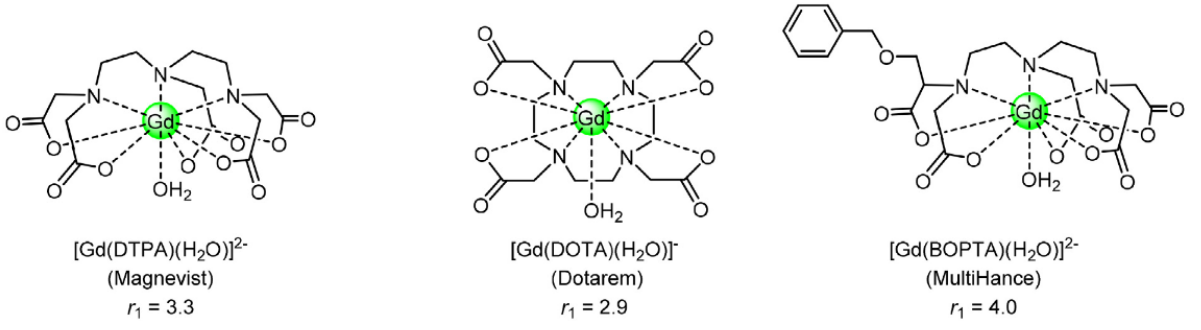


Figure 19.
Schematic representation of the molecular structure of some current commercially available $Gd^{3+}$ -containing MRI CAs. Charges in structures are omitted for clarity. The brand names are given between brackets. Relaxivities are in $s^{-1}$ $mM^{-1}$ measured in aqueous solution at 1.5 T and 37 ºC (BOPTA is a derivative of DTPA in which one $CH_2$ in the terminal methylene carboxylate group, $CH_2$–C(O)OH is replaced by $-CH_2-O-CH_2C_6H_5$).

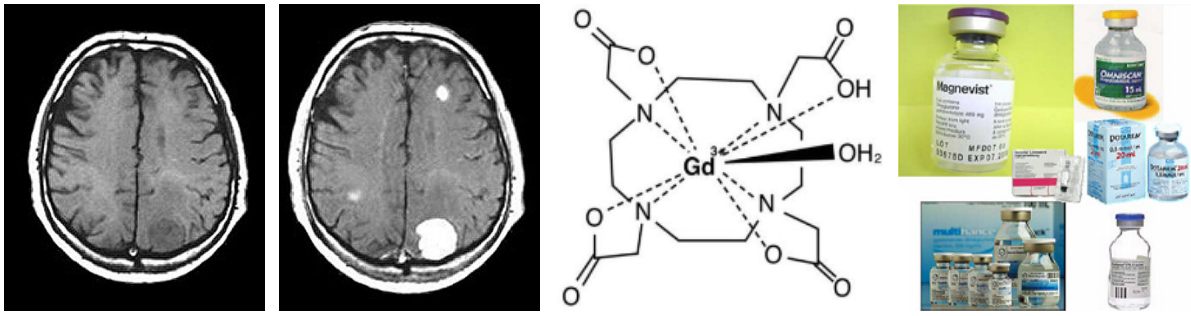


Figure 20.
From left to right: axial $T_{1w}$ MR image of a human patient with a brain tumour before and after (right) i.v. injection of a Gd-based MRI CA. The main tumour and some metastases are clearly visible as bright regions after addition of the CA; Chemical structure of $[Gd(DOTA)(H_2O)]^-$; clinical DOTAREM® (Guerbet).

Many stable paramagnetic $Ln^{3+}$ complexes have been developed as NMR shift and relaxation probes in various research areas, from studies of distribution of alkali metals in cells, tissues and *in vivo* animal organs, [36] to application as structural probes for small molecules [1, 43, 44, 48, 53] and as protein tags for structure and dynamics studies. [27]

$Ln^{3+}$ luminescent materials, including complexes, clusters, coordination polymers, ionic liquids, gels, metallomesogens, nanoparticles, in particular upconverting ones (UCNPs) and electroluminescent materials have found applications in the development of many high-technology devices. [5, 18, 28] Phosphors for displays and economical lighting, e.g. compact fluorescent lamps (CFLs) contain a phosphate mix that may include REEs such as $La^{3+}$ and $Y^{3+}$. Conventional phosphor-coated white light emitting diodes (LEDs), have been made by combination of individual red, green and blue LEDs or by conversion of blue or near UV light to lower energy emission by means of yellow-emitting phosphors, eg. yttrium aluminum garnet (YAG), or by combinations of blue, green and red phosphors coated on the semiconductor chip. [18] Organic light emitting diodes (OLEDs) with $Eu^{3+}$, $Tb^{3+}$ or $Sm^{3+}$-containing materials in the emission layers have also been described. [18] Upconverting phosphors (UCPs) are RE-doped ceramic-type materials (eg. oxides, oxysulfides, fluorides, oxyfluorides) which convert red light into visible light. They appear as microspheres or nanospheres (UCNPs), with many advantages, such as low sensitivity to photobleaching, high optical sensitivity due to the presence of many emitting centres per particle, capability for multiplex analyses due to the possible doping of different $Ln^{3+}$ ions, as well as cheap diode laser excitation (e.g. at 980 nm). Most of the UCNPs have $Y^{3+}$ as the carrier, $Er^{3+}$ as the emitter, since it has two emission lines in the green (540 nm) and in the red (654 nm), along with $Yb^{3+}$ as activator (eg. $Y_{0.86}Yb_{0.08}Er_{0.06}$), but other pairs such as $Tm^{3+}/Ho^{3+}$ have also been used. [18, 19]

REEs have applications in photocatalysis. Due to the variability of sunlight and to the difficulty of storing electricity, part of the harvested solar energy should be converted into chemical energy, which would then be available when needed. The easiest and most sustainable solution is splitting water by photolysis and storing energy in the simplest chemical bond, $H_2$. Photosynthesis can be achieved in solar water-splitting cells either by coupling a photovoltaic module to an electrolyser or accomplishing the splitting at the surface of a designed semi-conductor, which is simpler and more attractive. The splitting of one mole of water requires 237 kJ under standard conditions, which translates into a standard potential of 1.23 V. The semi-conductor must therefore absorb light with a wavelength $\lambda < 1$ μm and two

photons are required for producing one molecule of $H_2$ at the photocathode. However, in practice, losses cause the energy required for photoelectrolysis to be at least 1.6 eV per electron–hole pair generated, which translates into light with $\lambda < 775$ nm. For a dual bandgap system, solar-to-hydrogen conversion efficiencies on the order of 15% can be expected. Therefore, RE compounds are used as photoanode materials, for instance the perovskite $La_2Ti_2O_7$, or $Y_2Ti_2O_7$ and $Gd_2Ti_2O_7$ with pyrochlore-type structure. Another application of photocatalysis is the decomposition of air and water pollutants. Titanium oxide can remove a large number of organic pollutants, including chlorinated pollutants, but its large bandgap (3.2 eV) restricts its use to UV irradiation and lowering their bandgap is not easy because of the instability of doped $TiO_2$. Alternatives, such as $LaTaO_4$ are promising, as well as V–Ln–O composites which decompose acetone with 80% yield when Ln = $Gd^{3+}$. Another solution is to use $Ln^{3+}$ up-conversion, either by doping $TiO_2$ NPs with $Y_3Al_5O_{12}$: Er or by producing core-shell $YF_3$:Tm,Yb@$TiO_2$ NPs. Under solar illumination, 980 nm light is absorbed by $Yb^{3+}$ and up-converted by $Tm^{3+}$ which then emits at 290, 350, 360, 450, and 480 nm, that is in a range suitable for activating $TiO_2$. [9, 19]

REEs have applications in the electronic and photonic industries. [29] In electronics, NPO ceramic capacitors are single-layer ceramic capacitors produced by using a dielectric made of titanium dioxide ($TiO_2$) modified by magnesium oxide (MgO) (white ceramics) or a RE oxide, e.g. $Nd_2O_3$ (other NPO ceramics). NPO (Negative-Positive-Zero) is used to express the temperature characteristics. It shows that the capacitance temperature characteristic of NPO is very good, and the capacitance value does not drift with the change of positive and negative temperature.

The rapid development of telecommunication networks requires high speed digital data transmission, which travels through optical fibers as light with wavelengths in the 1000–1600 nm range. Optical amplifiers are basic elements of photonic integrated circuits (PIC), consisting of a microchip containing optical integrated components, such as amplifiers, splitters, couplers, multiplexers and de-multiplexers coupled to a laser source, which form a functioning circuit. This technology detects, generates, transports, and processes light. Although the transmission loss of the light passing through an optical fiber is very small (< 0.2 dB/km at light wavelength in the 1550 nm band), for long-distances (eg. 100 km) that transmission loss leads to extremely weak signals, which need to be amplified using an optical amplifier. Optical amplifiers amplify an optical signal directly, without the need to first convert it to an electrical signal. They are used as optical repeaters in the long distance fiberoptic cables which carry much of the world's telecommunication links. Among the major types of optical amplifiers, doped fiber amplifiers (DFAs) are optical amplifiers that use a doped optical fiber as a gain medium to amplify the incoming optical signal. [43] The signal to be amplified and a pump laser are multiplexed into the doped silica fiber, and the signal is amplified through interaction with the doping ions. They consist usually of a guiding layer with a high refractive index positioned between low refractive cladding layers. When the guiding layer is doped with active $Ln^{3+}$ ions, optical gain arises upon appropriate pumping. Some $Ln^{3+}$ are effective doping elements, especially $Er^{3+}$ (1530 nm), $Nd^{3+}$ (1060 nm), $Pr^{3+}$ (1300 nm) and $Tm^{3+}$ (1500 nm), as they show transitions in the range of telecommunication windows (1000–1600 nm). Erbium-doped fibre amplifiers (EDFAs) are much used. One of the limitations of EDFAs is the low absorption cross-section of $Er^{3+}$ f–f transitions and the other is concentration quenching. When the concentration of $Er^{3+}$ ions is larger than $10^{20}$ $cm^{-3}$, both excited state absorption and up-conversion considerably reduce the efficiency of the fibres. A solution is to use polymer fibres, for instance polymethylmethacrylate (PMMA) fibres, in which $Er^{3+}$ complexes with organic ligands are

doped. The resulting erbium-doped waveguide amplifiers (EDWAs) are optical amplifiers that use a waveguide to boost an optical signal. They have definite technical advantages over silica EDFAs: smaller size, better flexibility and larger core diameter which gives higher gain, as well as much lower pump threshold, allowing better coupling to local-scale splitters, couplers, and multiplexers, with easier integration in complex optoelectronic systems. The fabrication of new $Er^{3+}$-doped EDWAs has relied on SU-8 as cladding layer, purely inorganic fluoride nanoparticles, or $Er^{3+}$ complexes with organic ligands, for example, ternary $Er^{3+}$ dibenzoylmethanate with phen or $Er^{3+}$ nitrate with derivatives of triphenylphosphine oxide. [9, 18, 19]

REEs are also applied in electro-optics (EO), a branch of electronic engineering involving components, electronic devices such as lasers, laser diodes, LEDs, waveguides, etc. which operate by the propagation and interaction of light with various tailored materials. It is closely related with photonics. The electro-optic effect is a change in the optical properties of an optically active material due to the interaction with the electric field of light. This interaction usually results in a change in the birefringence, and not simply the refractive index of the medium. Mostly, the linear electro-optic effect (Pockels effect) is used, and less often the Kerr effect (quadratic electro-optic effect). The most important kind of electro-optic devices is the electro-optic modulator, containing a Pockels cell as its core element. Besides, the electro-optic effect can also be utilized in the form of electro-optic sampling. An example of electro-optic modulators are the high-quality lanthanum-modified lead zirconate titanate (PLZT) transparent thin films with an excellent theoretical quadratic EO coefficient, which have been fabricated by improved sol–gel techniques. [25]

In solar-energy conversion, sunlight can be directly converted into electricity in so-called solar (SC) or photovoltaic (PV) cells. The most widely used inorganic semiconductor for SC is silicon (Si). Interest in lanthanide-based materials for photon converting layers in SC stems from their unique luminescent properties with emission from UV to NIR spectral ranges. An example is the use of a $Ln^{3+}$-containing inorganic phosphor in down-shifting layers consisting of $Yb^{3+}$-doped glass ceramics containing $Ba_2TiSi_2O_8$ nanocrystals. Several up-converting materials, usually involving $Er^{3+}$, have been proposed for Si solar cells. [9, 18, 19]

The versatility of lanthanide luminescence, generated in inorganic materials or complexes with organic ligands upon visible or invisible (UV, NIR) excitation, makes these compounds ideal as active components in security inks, counterfeiting tags, or identifying codes. There are basically two types of luminescent security tags. The first one is based on down-conversion or down-shifting upon UV light excited luminescence. This is the case in euro bills for instance, which contain $Eu^{3+}$ (orange-red emission) and $Eu^{2+}$ (blue and green emission) phosphors (Figure 21). [54]


Figure 21.
Five Euro banknote (left) under white light and (right) under UV light. The europium salts in embedded fibers in the banknote fluoresce under UV light (from Wikimedia Commons)

Mixing different phosphors with different Ln ions and concentrations results in millions of potential combinations, an ideal situation for tagging all kind of products, from fabrics to explosives. The second type of tags uses mainly upconversion of the β-$NaYF_4$: Yb, Ln (Ln = Er, Tm) UCNPs. In the case of Ln = Er, the ratio of the red to green emission and the corresponding lifetimes can be tuned by varying the composition of the nanocrystals, their morphology and excitation power. This fine tuning allows to generate many potential combinations which can be used as unique identifying fingerprints. More combinations can be generated by mixing two types of NPs, eg. inks incorporating NPs doped with either $Er^{3+}$ or $Tm^{3+}$, capped with oleic acid and dissolved in toluene with poly(methyl)methacrylate as a binding agent, are proposed for printing quick response (QR) codes. (Figure 22). [10, 54]

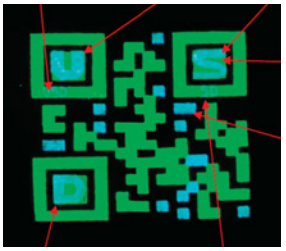

Figure 22.
Quick response (QR) codes using upconversion of the β-$NaYF_4$: Yb, Ln (Ln = Er, Tm) UCNPs.
Adapted from personal gift of Bünzli, J.-C. G.

Lanthanide luminescence materials have many applications in bioanalyses and in cell, tissue and animal optical imaging. Bioanalyses with $Ln^{3+}$ luminescent sensors operating usually in water, are of two types: i) the sensor is immobilized, e.g. in silicon thin layers directly integrated into an electronic readout circuit; ii) classical luminescent probes in solution for *in vitro* and/or *in vivo* applications. In the second case, the emitted signal has to be normalized to another signal to avoid concentration dependence (ratiometric method). New biosensors use more sensitive probes based on nanostructures and exploit the time-resolved capability of $Ln^{3+}$ luminescent bioprobes. [7, 8]

In heterogeneous immunoassays, time-resolved detection is applied due to the many undesirable substances coexisting in blood serum or in urine. Two $Ln^{3+}$ chelates are used in the commercial procedure (dissociation-enhanced lanthanide fluorometric immunoassay -DELFIA). The analyte is linked to a specific binding agent immobilized on a solid support, followed by coupling of a poorly luminescent $Ln^{3+}$ complex with the analyte by another specific immunoreaction, the unreacted reagents are washed out and the chelate is dissociated in acidic medium and converted into another, highly luminescent complex protected by a micelle thanks to an enhancement solution. (Figure 23, left). Finally, time-resolved detection of the metal-centered luminescence yields the desired analytical signal. Antigens (e.g., hepatitis B surface antigen), steroids (e.g., testosterone or cortisol) and hormones (e.g., luteinizing (LH) and follicle stimulating (FSH) hormones, Figure 23, right, top left) are routinely assayed with this heterogeneous technique. Improved one step dual-label assays are used for analysis of free and bound prostate specific antigen (PSA) (Figure 23, right, top right), the concentration of which increases in prostate cancer patients. Homogeneous assays (homogeneous time-resolved fluorescence - HTRF) are based on direct modulation of the label luminescence during the biochemical reaction under study. The antigen of interest is coupled to two mAbs, one decorated with a $Ln^{3+}$ label and the other one with an organic acceptor emitting at a wavelength distinct from the $Ln^{3+}$ emission (Figure 23, right, bottom left).[7] After the immunoreactions are completed, the sample is illuminated by UV light and four types of luminescence develop: (i) two

fast decaying signals, background autofluorescence and fluorescence from the organic conjugate not bound to the antigen, and (ii) two slow decaying emissions, phosphorescence from the $Ln^{3+}$ conjugate not bound to the antigen and emission from the organic acceptor bound to the antigen and excited through FRET (Fluorescence Resonance Energy Transfer). The transfer depends, according to Förster's law, on the donor (D)- acceptor (A) distance, $R_{DA}$, as $(R_{DA})^{-6}$, on a proper alignment between the two moieties, substantial spectral overlap integral ($J_{DA}$) between the emission spectrum of the donor and the absorption spectrum of the acceptor. [8] Measurement in time-resolved mode allows to eliminate the fast decaying background luminescence signals and spectral discrimination isolates the signal from the organic acceptor fed by the FRET process. This technique avoids removal of the unreacted conjugates and reduces the analysis time, making this technique, adequate for high throughput screening operations. TR homogeneous assays have been commercialized under the trademark HTRF from CisBio International® using a stable $Eu^{3+}$-tris(bipyridine) cryptate (Figure 23, right, bottom right). The FRET technology and heterogeneous immunoassays, have been successfully applied in many areas of *in vitro* biosciences, such as time-resolved luminescence flow cytometry, DNA hybridization assays, detection of enzyme activity for diagnosis of diseases like cancer, real-time polymerase chain reactions (PCR) and genotyping.

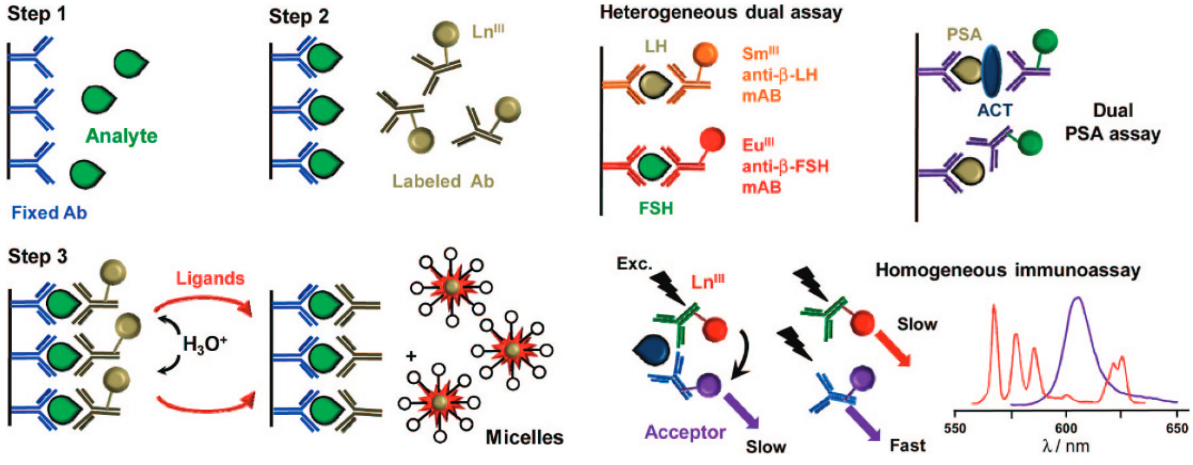


Figure 23.
Left: Principle of an heterogeneous luminescent immunoassay (Ab= antibody): fixation of the analyte (step 1), immunochemical reaction with the labelled antibody (step 2), release of $Ln^{3+}$ followed by complexation and insertion into micelles (step 3); Right: (top left) heterogeneous dual assay of luteinizing (LH) and follicle stimulating (FSH) hormones with $Sm^{3+}$ and $Eu^{3+}$ bioconjugates; (top right): dual assay of free and bound PSA; (bottom left): principle of an homogeneous immunoassay showing time (slow/fast) and spectral discrimination of the unreacted monoclonal antibodies; (bottom right): emission spectra of a $[Eu(cryptate)_3]$ in red and of XL665 in violet. Reprinted from ref. 7 with permission. Copyright 2010, American Chemical Society.

Lanthanide luminescent bioprobes (LLBs) responsive to pH, phosphate, enzyme activity, redox state biomarkers (singlet oxygen ($^1O_2$), $H_2O_2$), etc. have also been reported, as well as for detection and quantification of simple analytes. [7, 11, 19] LLBs can also be used in solution by bioconjugation of the $Ln^{3+}$ chelate with an activated group to react with a functional group of a bioactive molecule for bio-analysis.

Another, completely different analytical tool is Lanmodulin (LanM), a highly selective $Ln^{3+}$-binding protein, which possesses four metal binding EF hand motifs, commonly associated with $Ca^{2+}$-binding proteins. It has been developed into a sensor that can identify $Tb^{3+}$ from complex environments, such as acid mine drainage. The sensor, illustrated in Figure 24, emits green light when bound to $Tb^{3+}$. [20]

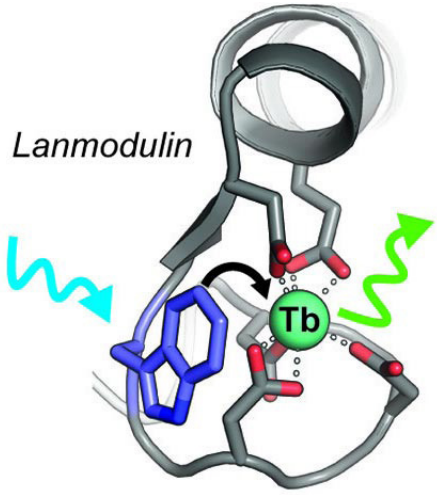


Figure 24.
Structure of $Tb^{3+}$- Lanmodulin, a sensor for luminescent $Tb^{3+}$. Reprinted from ref. 20 with permission. Copyright 2021, American Chemical Society.

Up-converting nanoparticles (UCNPs) are excellent reporters in the visible and NIR, and their targeted bioconjugates have performances for bio-assays comparable to those of $Eu^{3+}$-based labels. [8, 9, 19] Some of the analyses described here require sophisticated instrumentation and/or data treatment and are not easily transferable to point-of-care technology. Lateral-flow paper biosensors are appealing and cheap for detection of human and veterinary disease pathogens, as well as for food quality control and identification of drug abuse. Systems biology requires monitoring very large numbers of samples through high--throughput and multiplex protocols. Miniaturization linked to robotics and efficient data treatment provides the necessary technology for meeting this requirement, which can be achieved by microarrays. [8]

The properties of LLBs makes them ideal for visible and NIR fluorescence cell, tissue and small animal optical imaging. As many $Ln^{3+}$ complexes are cell-permeable, the unique spectroscopic properties of LLBs have been used to obtain images of cells, for instance in the follow up of cancer therapy, using time-resolved detection in microscopy. LLBs can also detect and quantify many important analytes (e.g., $Ca^{2+}$, bicarbonate, ascorbate, urate) and their fluctuations with high spatial resolution, yield very important information on cellular metabolism. These optical probes can be specifically modified or bioconjugated to know where these molecules accumulate in live cells and what their concentrations are in the various cell organelles. An example is Parker's study of over 60 different cyclen-based $Eu^{3+}$ and $Tb^{3+}$ LLBs containing various chromophores, such as tetraazatriphenylenes, acridones, azaxanthones, azathiaxanthones, or pyrazolyl azaxanthones, for target cell optical imaging (OI). This work established that the nature of the chromophore and its attachment mode to the macrocycle primarily determines the cell uptake and localization and not the charge of the complex or its lipophilicity [38, 39] (Figure 25). UCNPs bioconjugates are very successful LLBs for bioimaging. Binuclear, self-assembled lanthanide helicates $[Ln_2L_3]$ with hexadentate ligands derived from bis(benzimidazole)pyridine building blocks, which act both as strongly coordinating groups and efficient sensitizing units, have also been proposed as LLBs. The luminescence of both $Eu^{3+}$ and $Tb^{3+}$ is substantially sensitized and they are non-cytotoxic for several human cell lines, while penetrating into them by endocytosis, so that time-resolved luminescence imaging is feasible. Further derivatization leads to helicates (Ln = Eu, Tb) which can be bioconjugated to either avidin or monoclonal antibodies. In this way, biomarkers expressed by cancerous cells can be specifically detected,

allowing distinction between cancerous and non-cancerous cells. The specificity of these bioconjugates was useful for simultaneous detection of two biomarkers expressed by human breast cancer cells, the estrogen receptors (ER) located on the nucleus membrane and the human epidermal growth factor receptors (Her2/neu) lying on the cell membrane. [7, 18, 19] (Figure 26).

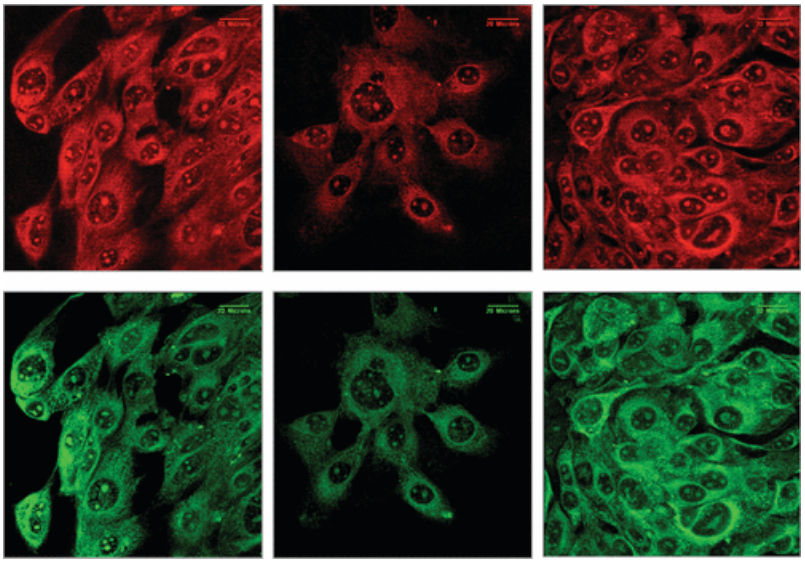

Figure 25.
Confocal microscopy images ($\lambda_{exc}$ = 405 nm) showing the intracellular localization profile of a typical europium–azathiaxanthone complex (green, ligand fluorescence; red, Eu emission), highlighting its distribution in the protein-dense nucleoli (bright spots, center) and ribosomes. Reprinted from ref. 38 with permission. Copyright 2009, American Chemical Society.

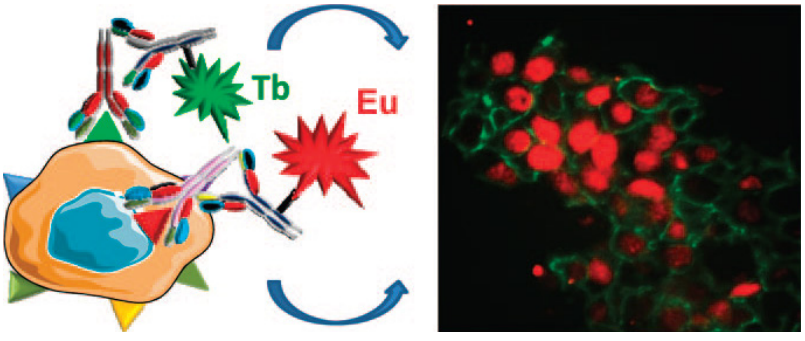


Figure 26.
(Left) Principle of the lab-on-a-chip dual assay for estrogen receptors (nucleus) and human epidermal growth factor receptors (cell membrane) with binuclear $Ln^{III}$ helicates $[Ln_2(L43c)_3]^{3-}$ conjugated to specific antibodies. (Right) Time resolved microscopy of a breast cancer tissue section pressed into a 100 µm wide microchannel. Reprinted from ref. 7 with permission. Copyright 2010, American Chemical Society.

The current development of LLBs for visible and NIR fluorescence cell, tissue and small animal imaging, includes developing bimodal imaging probes for simultaneous OI/MRI, combining the sensitivity of OI with the penetration and image resolution of MRI, eg. by tailoring of dual-probe UCNPs, [10] the design of responsive LLBs and NPs, eg. for pH and temperature sensing, allowing pH and temperature

mapping of cells and tissues [10, 19, 24], and circularly polarized luminescence (CPL) bioprobes based on $Ln^{3+}$ complexes with chiral linear, tripodal and tetrapodal ligands. [11, 41] In this respect, a CPL Laser Scanning Confocal Microscope (CPL-LSCM) was developed capable of simultaneous chiroptical contrast based live-cell imaging of endogenous and engineered CPL-active cellular probes. [50] Live small animal imaging is a challenge due to the limited penetration depth of light through tissues. The bulk of *in vivo* bioimaging studies have used NIR excitation and emission using NIR–NIR UCNPs and $Er^{3+}$. An example is the acquisition of *in vivo* whole-body images of a nude mouse subcutaneously injected with ligand-free ($NaGdF_4$:3%Nd)/$NaGdF_4$ nanocrystals. [8]

A futuristic vision in nanomedicine is to provide nanorobots for *in vivo* advanced diagnosis, medical therapies, and minimally invasive surgery. These nanorobots integrate embedded nanoelectronics and circuits to sense their environment, for instance for determining local temperature, pH, or concentrations of analytes in blood. [10] They require an adequate source of electrical energy. One of the proposed solutions takes advantage of the large transparency of biological tissues to NIR light in the production of electricity from conversion of NIR light by photovoltaic cells. A device with hydrophilic nanophosphors NaY-$F_4$: Er (2%),Yb (20%) was prepared via one-step hydrothermal synthesis and its biological compatibility was optimized with a stable succinonitrile-based gel electrolyte. In this device, 93% of the upconverted light is absorbed by the organic dye. Under irradiation with a 980 nm laser delivering 1W power, the yield of laser-to-electricity conversion was 0.09%. With skin-safe 720 mW $cm^{-2}$ illumination, the device had a maximum output power of 44.5 mW, corresponding to $\eta_{l-e}$ = 0.039%. The output power reduced to 22.2 mW ($\eta_{l-e}$ = 0.019%) when the cell was covered with 1 mm layer of chicken skin as a model for biological tissues. Although small, this power is sufficient to energize devices fabricated with nanowires or nanotubes, possible nanorobots for *in vivo* advanced diagnosis, medical therapies, and minimally invasive surgery. [8]

Many objects around us contain REs, such as cars, smart cell phones, electronic displays, fluorescent lamps, light emitting diodes (LEDs), optical fibres, micro-motors, medical scanners, among others and military applications, such as night vision goggles, radiation detectors, sonar, electronic warfare jamming devices, guidance and control in avionics and drones and laser weapons. Cars have typically 8-12 kg of REs, present in various parts, from electric motors and generators to hybrid batteries (Figure 27).

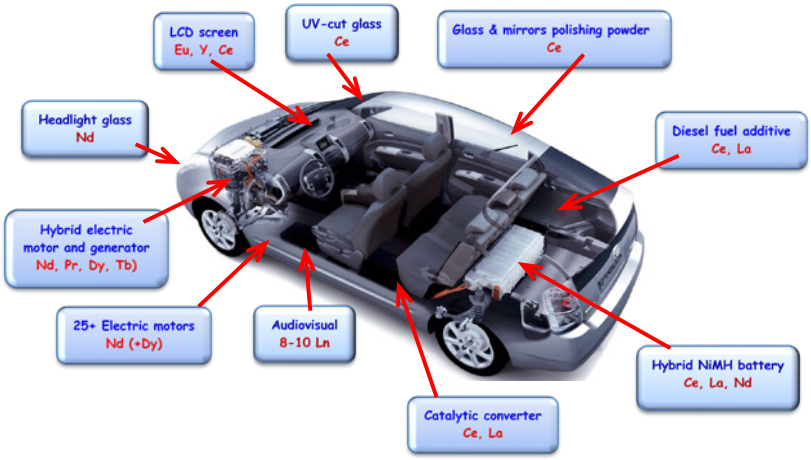


Figure 27.
Parts of an electric car containing REEs. Adapted from personal gift of Bünzli, J.-C. G.

Smart cell phones have 150-250 mgs of nine REEs, in a variety of parts: screen, circuitry, speakers, buzzer and polishing (Figure 28).

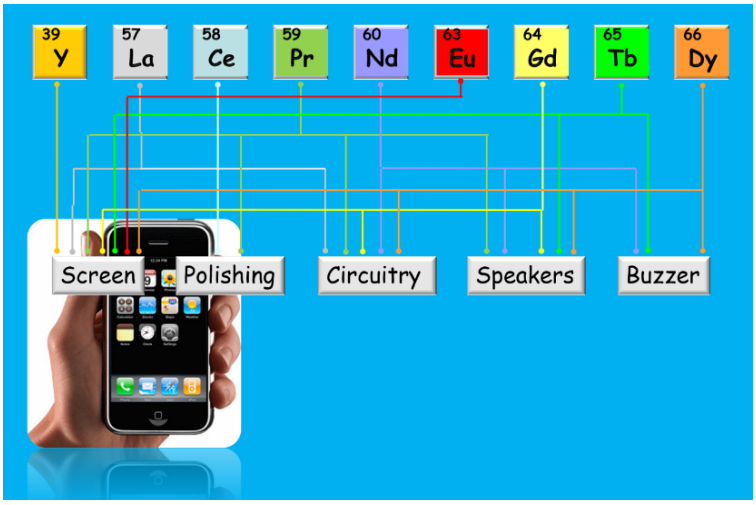


Figure 28.
REEs in a smart phone and their function. Adapted from personal gift of Bünzli, J.-C. G.

## 4. CONCLUSIONS

Rare earths are a group of 17 chemically similar elements crucial to the manufacture of many high--technology products. Despite their name, most are abundant in nature but are hazardous to extract. Most REEs have uses in several different fields and are present in many objects around us. We rely on REEs to colour our smartphone screens, fluoresce to signal authenticity in euro banknotes and relay signals through fiber-optic cables across the seafloor. They are also essential for building some of the world's strongest and most reliable magnets. They generate sound waves in headphones, boost digital information through space and shift the trajectories of heat-seeking missiles. REEs are also driving the growth of green technologies, such as solar and wind energy and electric vehicles, and may even give rise to new components for quantum computers. While conventional computers use binary bits (those 1s and 0s), quantum computers use qubits, which can occupy two states simultaneously. Crystals containing REEs make good qubits, since the shielded f-electrons can store quantum information for long periods of time. One day, computer scientists might even use the luminescent properties of REEs in qubits to share information between quantum computers and give birth to quantum internet. Applications in geochemistry, including radioanalytical methods, catalysis, biosciences and medicine are many, including lasers for surgery and NIR-emitting $Ln^{3+}$ UCNPs as OI/MRI probes for *in vivo* animal imaging and therapy and radioisotopes for animal and human Positron Emission Tomography (PET) imaging and radiotherapy. It may be too early to predict exactly how the RE metals will continue to influence the expansion of these growing technologies, but it is probably safe to say: "We are going to need more rare earths".

(Comunicação apresentada à Classe de Ciências
na sessão de 20 de Outubro de 2022)

## REFERENCES


1. Aime, S., Barge, B., Delli Castelli, D., Fedeli, F., Mortillaro, A., Nielsen, F. U., & Terreno, E. Paramagnetic Lanthanide(III) complexes as pH-sensitive chemical exchange saturation transfer (CEST) contrast agents for MRI applications, Magn. Reson. Med. 47, 639 – 648 (2002); https://doi.org/10.1002/mrm.10106
2. Aneggi, E., de Leitenberg, C., Boaro, M., Fornasiero, P. & Trovarelli, A. "Catalytic applications of cerium dioxide" in *Cerium Oxide ($CeO_2$): Synthesis, Properties and Applications*, Scirè, S., Palmisano, L. (eds.), Elsevier, 2020, pp. 45-108
3. Balaram, V., Rare earth elements: A review of applications, occurrence, exploration, analysis, recycling, and environmental impact. Geoscience Frontiers, 10, 1285-1303, (2019); http://dx.doi.org/10.1016/j.gsf.2018.12.005
4. Binnemans, K., Jones, P. T., Müller, T. & Yurramendi, L. Rare earths and the balance problem: How to deal with changing markets? Journal of Sustainable Metallurgy. 4, 126–146 (2018); http://dx.doi.org/10.1007/s40831-018-0162-8.
5. Brunckova, H., Rocha, L. A., Nassar, E. J., Moscardini, S. B. & Kolev, H. Luminescence properties of neodymium, samarium, and europium niobate and tantalate thin films, Luminescence, 37, 642-655 (2022); https://doi.org/10.1002/bio.4205
6. Bünzli, J.-C. G., "Lanthanides", in *Kirk-Othmer Encyclopedia of Chemical Technology*, Kirk-Othmer (ed) Wiley, 2013, pp. 1-49; https://doi.org/10.1002/0471238961.1201142019010215.a01.pub3
7. Bünzli, J.-C. G. Lanthanide Luminescence for Biomedical Analyses and Imaging, Chem. Rev., 110, 5, 2729–2755 (2010); https://doi.org/10.1021/cr900362e
8. Bünzli, J.-C. G. Lanthanide light for biology and medical diagnosis, J. of Luminescence, 170, 866-878 (2016); https://doi.org/10.1016/j.jlumin.2015.07.033
9. Bünzli, J.-C. G. &. Eliseeva, S. V., Lanthanide NIR luminescence for telecommunications, bioanalyses and solar energy conversion, J. of Rare Earths, 28, 824-842 (2010); https://doi.org/10.1016/S1002-0721(09)60208-8
10. Bünzli, J.-C. G. &. Eliseeva, S. V., Intriguing aspects of lanthanide luminescence, Chem. Sci., 4, 1939-1949 (2013); https://doi.org/10.1039/C3SC22126A
11. Bünzli, J.-C. G. & Piguet, C. Taking advantage of luminescent lanthanide ions, Chem. Soc. Rev. 34, 1048–1077 (2005); https://doi.org/10.1039/b406082m
12. Calestani, G. &. Rizzoli, C. Crystal structure of the $YBa_2Cu_3O_7$ superconductor by single-crystal X-ray diffraction, Nature, 328, 606–607 (1987); https://doi.org/10.1038/328606a0
13. Caravan, P., Ellison, J. J., McMurry, T. J. & Lauffer, R. B. Gadolinium(III) Chelates as MRI Contrast Agents: Structure, Dynamics, and Applications, Chem. Rev. 99, 2293–2352 (1999); https://doi.org/ 10.1021/cr980440x
14. Choppin, G. R., "Chemical properties of the rare earth elements", in *Lanthanide probes in life, chemical and earth sciences*, Bünzli, J.-C. G., Choppin, G. R. (eds)., Elsevier, Amsterdam, 1989, Ch. 1, pp. 1-41.
15. Chow, C. Y., Eliseeva, S. V., Trivedi, E. R., Nguyen, T. N., Kampf, J. W., Petoud, S. & Pecoraro, V. L. $Ga^{3+}/Ln^{3+}$ Metallacrowns: A Promising Family of Highly Luminescent Lanthanide Complexes That Covers Visible and Near-Infrared Domains J. Am. Chem. Soc. 138, 5100–5109 (2016); http://dx.doi.org/10.1021/jacs.6b00984
17. D'Angelo, P., Zitolo, A., Migliorati, V., Chillemi, G., Duvail, M., Vitorge, P., Abadie, S. & Spezia, R. Revised Ionic Radii of Lanthanoid (III) Ions in Aqueous Solution, Inorg. Chem. 50, 4572–4579 (2011); http://dx.doi.org/10.1021/ic200260r
18. Eliseeva, S. V. & Bünzli, J.-C. G. Lanthanide luminescence for functional materials and bio-sciences, Chem. Soc. Rev., 39, 189-227 (2010); https://doi.org/10.1039/b905604c
19. Eliseeva, S. V. & Bünzli, Rare earths: jewels for functional materials of the future, New J. Chem., 35, 1165–1176 (2011); https://doi.org/10.1039/c0nj00969e
20. Featherston, E. R., Issertell, E. J. & Cotruvo Jr., J. A. Probing Lanmodulin's Lanthanide Recognition via Sensitized Luminescence Yields a Platform for Quantification of Terbium in Acid Mine Drainage, J. Am. Chem. Soc., 143, 14287−14299 (2021) https://doi.org/10.1021/jacs.1c06360
21. Geijer, B. R., Crells Chem. Ann. 229–230 (1788)
22. Geraldes, C.F.G.C. & Laurent, S. Classification and basic properties of contrast agents for magnetic resonance imaging, Contrast Media & Molecular Imaging 4, 1-23 (2009); https://doi.org/10.1002/cmmi.265
23. Haxel, G. B., Hedrick, J. B., Orris, G. J., Rare Earth Element Resources: A Basis for High Technology, U.S. Geological Survey Fact Sheet 087-02, 2002
24. Heffern, M.C., Matosziuk, L.M & Meade, T.J. Lanthanide Probes for Bioresponsive Imaging, Chem. Rev. 114, 4496–4539 (2014); https://doi.org/10.1021/cr400477t

25. Huang, C., Li, D., He, T., Peng, Y., Zhou, W., Yang, Z., Xu, J. & Wang, Q. Large Quadratic Electro-Optic Effect of the PLZT Thin Films for Optical Communication Integrated Devices, ACS Photonics, 7, 3166–3176 (2020); https://doi.org/10.1021/acsphotonics.0c01234
26. Ishikawa, N., Sugita, M., Ishikawa, T., Koshihara, S.-y. & Kaizu, Y. Lanthanide Double-Decker Complexes Functioning as Magnets at the Single-Molecular Level, J. Am. Chem. Soc. 125, 8694-8695 (2003); https://doi.org/10.1021/ja029629n
27. Keizers, P. H. J. & Ubbink, M. Paramagnetic tagging for protein structure and dynamics analysis, Progr. Nuclear Magnetic Resonance Spectrosc., 58, 88-96 (2011); https://doi.org/10.1016/j.pnmrs.2010.08.001
28. Khan, L.U. & Khan, Z.U. Rare Earth Luminescence: Electronic Spectroscopy and Applications, in S. Sharma (ed.) Handbook of Materials Characterization, Springer, Cham., 2018; https://doi.org/10.1007/978-3-319-92955-2_10
29. Kilburn, B. T. The role of the lanthanides in the photonics, electronics and related industries, Inorg. Chim. Acta, 140, 335-338 (1987); https://doi.org/10.1016/S0020-1693(00)81117-2
30. Kumari, A., Panda, R., Jha, M. K., Kumar, M. K. & Lee, J. Y., Process development to recover rare earth metals from monazite mineral: A review, Minerals Engineering 79, 102–115 (2015) http://dx.doi.org/10.1016/j.mineng.2015.05.003
31. Kurzen, H., Bovigny, L., Bulloni, C. & Daul, C, Electronic structure and magnetic properties of lanthanide 3+ cations, Chem. Phys. Lett., 574, 129–132 (2013) https://doi.org/10.1016/j.cplett.2013.04.070
32. Liu, G., *Electronic Energy Level Structure*, in Spectroscopic properties of rare earths in optical materials, Chapter 1, Liu, G., Jacquier, B. (eds.), in Springer Series in Materials Science, Hull, R., Osgood Jr., Parisi, R., J., Warlimont, H. (eds.), Vol. 83, Springer, 2005.
33. Lucas, J., Lucas, P., Le Mercier, T., Rollat, A., Davenport, W. W. (eds.), *Rare Earths - Science, Technology, Production and Use*, Elsevier, 2015
34. Luong, J. H. T., Tran, C. & Ton-That, D. Energies 15, 7997(2022); https://doi.org/10.3390/en15217997
35. Luzon, J. & Sessoli, R. Lanthanides in molecular magnetism: so fascinating, so challenging, Dalton Trans.,41, 13556–13567 (2012); https://doi.org/10.1039/c2dt31388j
36. Malloy, C. R., Buster, D. C., Castro, M. M. C. A., Geraldes, C. F. G. C., Jeffrey, F. M. H. & Sherry, A. D. Influence of global ischemia on intracellular sodium in the perfused rat heart, Magn. Reson Med., 15, 33-44, (1990); https://doi.org/10.1002/mrm.1910150105
37. Min, P., Zhang, S., Xu, Y. Enhanced oxygen storage capacity of $CeO_2$ with doping-induced unstable crystal structure, *Appl. Surface Sci.*, 448, 435-4431 (2018); https://doi.org/10.1016/j.apsusc.2018.04.103
38. Montgomery, C. P., Murray, B. S., New, E. J., Pal, R. & Parker, D., Cell-Penetrating Metal Complex Optical Probes: Targeted and Responsive Systems Based on Lanthanide Luminescence, Acc. Chem. Res., 42, 925-937 (2009); https://doi.org/10.1021/ar800174z
39. New, E. J., Parker, D., Smith, D. G. & Walton, J. W. Development of responsive lanthanide probes for cellular applications, Curr. Opinion Chem. Biol., 14, 238–246 (2010); https://doi.org/10.1016/j.cbpa.2009.10.003
40. Olabi, A. G. & Grunwald, A. Design and application of magnetostrictive materials, Materials & Design, 29, 469-483, (2008); https://doi.org/10.1016/j.matdes.2006.12.016
41. Parker, D., Fradgley, J. D. & Wong, K.-L. The design of responsive luminescent lanthanide probes and sensors, Chem. Soc. Rev., 50, 8193–8213 (2021); https://doi.org/10.1039/d1cs00310k
42. Parker, D. & Williams, J. A.G. Getting excited about lanthanide complexation chemistry, J. Chem. Soc. Dalton Trans. 3613–3628 (1996); https://doi.org/10.1039/DT9960003613
43. Pearsall, T. *Photonics Essentials*, 2nd edition, New York, McGraw-Hill, 2010
44. Peters, J. A., Huskens, J. D. & Raber, J. Lanthanide induced shifts and relaxation rate enhancements, Progr. Nuclear Magnetic Resonance Spectrosc., 28, 283-350 (1996); https://doi.org/10.1016/0079-6565(95)01026-2
45. Pyykkö, P. & Orama, O., "What did Johan Gadolin Actually do?", in *Episodes from the History of the Rare Earth Elements*, Evans, C. H. (ed), Kluwer Academic Publishers, 1996, pp,1-12; http://dx.doi.org/10.1007/978-94-009-0287-9
46. Ready, J. F., *Industrial Applications of Lasers*, London, Academic Press, 1997
47. Shannon, R. D. Revised Effective Ionic Radii and Systematic Studies of Interatomic Distances in Halides and Chaleogenides, Acta Crystallogr., A32, 751–767 (1976)
48. Sherry, A. D. & Geraldes, C. F. G. C. "Shift reagents in NMR spectroscopy", in *Lanthanide probes in life, chemical and earth sciences*, Bünzli, J.-C. G., Choppin, G. R. (eds), Elsevier, Amsterdam, 1989, Ch. 4, pp. 93-126.
49. Skomski, R. & Sellmyer, D.J. Anisotropy of rare-earth magnets, J. of Rare Earths, 27, 675- 679 (2009); https://doi.org/10.1016/S1002-0721(08)60314-2

50. Stachelek, P., MacKenzie, L., Parker, D. & Pal, R. Circularly polarised luminescence laser scanning confocal microscopy to study live cell chiral molecular interactions, Nature Commun.,13, 553 (2022); https://doi.org/10.1038/s41467-022-28220-z
51. Suli, L. M., Ibrahim, W. H. W., Aziz, B. A.; Deraman, M. R. & Ismail, N. A., A review of rare earth mineral processing technology, Chem. Eng. Res. Bull. 19, 20-35 (2017)
52. Suturina, E. A., Mason, K., Geraldes, C. F. G. C., Chilton, N. F., Parker, D. & Kuprov, I. Lanthanide-induced relaxation anisotropy Phys. Chem. Chem. Phys., **20**, 17676 – 17686 (2018); https://doi.org/10.1039/c8cp01332b
53. Suturina, E. A., Mason, K., Geraldes, C. F. G. C., Kuprov, I. & Parker, D. Beyond Bleaney's Theory: Experimental and Theoretical Analysis of Periodic Trends in Lanthanide-Induced Chemical Shift, Angewandte Chem. Int. Ed., **56**, 12215-12218 (2017); https://doi.org/10.1002/ange.201706931
54. Suyver, J. F. & Meijerink, A. Europium safeguards the euro, Chemisch2Weekblad, Vol. 98-4, February 16, 2002, p. 12.
55. Takaya, Y., Yasukawa, K., Kawasaki, T., Fujinaga, K., Ohta, J. et. al, The tremendous potential of deep-sea mud as a source of rare-earth elements, Sci. Rep., 8, 5763 (2018) http://dx.doi.org/10.1038/s41598-018-23948-5
56. Thyssen, P. & Binnemans, K., "Accommodation of the rare earths in the periodic table: A historical analysis", in *Handbook of Physics and Chemistry of Rare Earths*, Gschneider, Jr., K. A., Bünzli, J.-C. G., Pecharsky, V. K. (eds), Elsevier, 2011, Vol. 41, Chapter 248, pp. 1–93
57. Tommasi, F., Thomas, P. J., Pagano, G., Perono, G. A., Oral, R., Lyons, D. M., Toscanesi, M. & Trifuoggi, M. Review of Rare Earth Elements as Fertilizers and Feed Additives: A Knowledge Gap Analysis, Archives of Environmental Contamination and Toxicology, 81, 531–540 (2021); https://doi.org/10.1007/s00244-020-00773-4
58. Tóth, É., Helm, L., Merbach, A. E. (eds) *Chemistry of Contrast Agents in Medical Magnetic Resonance Imaging*; 2nd ed.; John Wiley & Sons Ltd: Chichester, 2013
59. Vikram, L. & Sivasankar, B. N. New nine coordinated hydrated heavier lanthanide ethylenediaminetetraacetates containing hydrazinium cation: Crystal structure of $N_2H_5[Dy(EDTA)(H_2O)_3](H_2O)_5$, Indian J. Chem., 47A, 25-31 (2008)
60. Vladimirov, Y. A., Osipov, A. N. & Klebanov, G. I. Photobiological Principles of Therapeutic Applications of Laser Radiation, Biochemistry (Moscow), 69, 81-90 (2004)
61. Vojtísek, P.; Cígler, P., Kotek, J., Rudovsky, J., Hermann, P. & Lukes, I. Crystal Structures of Lanthanide (III) Complexes with Cyclen Derivative Bearing Three Acetate and One Methylphosphonate Pendants, P. Vojtísek, P. Cígler, J. Kotek, J. Rudovsky, P. Hermann, I. Lukes, Inorg. Chem. 44, 5591–5599 (2005); http://dx.doi.org/10.1021/ic048190s
62. Weissman, S. I. Intramolecular energy transfer the fluorescence of complexes of europium, J. Chem. Phys. 10, 214–217 (1942); https://doi.org/10.1063/1.1723709
63. Wahsner, J., Gale, E. M., Rodríguez-Rodríguez, A. & Caravan, P. Chemistry of MRI Contrast Agents: Current Challenges and New Frontiers Chemistry of MRI Contrast Agents: Current Challenges and New Frontiers, Chem. Rev. 119, 2, 957–1057 (2019); https://doi.org/10.1021/acs.chemrev.8b00363